frontiers | Frontiers in Earth Science

TYPE Original Research
PUBLISHED 16 July 2025
DOI 10.3389/feart.2025.1602273

Check for updates

OPEN ACCESS

EDITED BY
Andrew La Croix,
University of Waikato, New Zealand

REVIEWED BY
Mumtaz Ali Khan,
Bahria University, Pakistan
Imad Mahmood Ghafor,
University of Sulaymaniyah, Iraq
Hamad Ur Rahim,
Pakistan Museum of Natural History, Pakistan
Merve Ozyurt,
Karadeniz Technical University, Türkiye

*CORRESPONDENCE
Huaguo Wen,
wenhuaguo08@cdut.edu.cn

RECEIVED 29 March 2025
ACCEPTED 23 June 2025
PUBLISHED 16 July 2025

CITATION
Chen S, Wen H, Li X, Huo F, Mo B, Liang J and Duan L (2025) Influence of structural setting, depositional environment and differential diagenesis on reservoir quality of the Xixiangchi formation in the central and southern Sichuan Basin, China. *Front. Earth Sci.* 13:1602273. doi: 10.3389/feart.2025.1602273

Influence of structural setting, depositional environment and differential diagenesis on reservoir quality of the Xixiangchi formation in the central and southern Sichuan Basin, China

Shizhen Chen[1,2,3], Huaguo Wen[1,2,3]*, Xiang Li[1,2,4], Fei Huo[5], Bowen Mo[1,2,3], Jintong Liang[1,2,3] and Lian Duan[1,2,3]

[1]State Key Laboratory of Oil and Gas Reservoir Geology and Exploitation, Chengdu University of Technology, Chengdu, China, [2]Key Laboratory of Deep-time Geography and Environment Reconstruction and Applications of Ministry of Natural Resources, Chengdu University of Technology, Chengdu, China, [3]Institute of Sedimentary Geology, Chengdu University of Technology, Chengdu, China, [4]College of Earth and Planetary Sciences, Chengdu University of Technology, Chengdu, China, [5]School of Geoscience and Technology, Southwest Petroleum University, Chengdu, China

The Middle-Upper Cambrian Xixiangchi Formation (504 - 488 Ma) dolomite in the central-southern Sichuan Basin constitutes significant hydrocarbon reservoirs, though their complex genetic mechanisms remain inadequately constrained. This study investigates dolomite types within the Xixiangchi Formation through petrography, physical property analysis, and geochemical analyses (C - O isotopes, rare earth elements) to elucidate reservoir characteristics and diagenetic evolution. Reservoir lithologies comprise four dolomite types: microcrystalline dolomite (≤31 μm, D1), fabric-retentive dolomite (<100 μm, D2), very finely to finely crystalline dolomite (31 ~ 100 μm, D3), and finely to medium crystalline dolomite (100 ~ 300 μm, D4). All dolomite types exhibit rare earth element patterns and isotopic signatures (δ^{13}C: –1.39‰ ± 0.67‰ to - 1.23‰ ± 0.71‰; δ^{18}O: –8.62‰ ± 1.18‰ to - 8.15‰ ± 0.98‰) comparable to coeval micritic limestones, indicating formation from evaporatively-concentrated seawater or marine-derived fluids. D1 displays laminated textures with relatively elevated δ^{18}O values and minimal Fe-Mn concentrations, consistent with near-surface precipitation. D2 exhibits coarser grain size, reduced Ce anomaly intensity (0.92 ± 0.06) compared to micritic dolomite, and lower δ^{18}O values, indicating its formation during shallow-to-moderate burial diagenesis, possibly associated with downward percolation-reflux of Mg^{2+}-rich evaporative brines. D3 and D4 show mosaic contact and granular phantom textures, along with lower Ce anomaly intensities (0.93 ± 0.05, 0.91 ± 0.6) and decreased total rare earth element contents, which imply a deeper diagenetic environment than that of D2. Genetic analysis reveals D1-D2 originated through penecontemporaneous evaporative dolomitization and shallow reflux processes, while D3 - D4 formed via burial dolomitization and dolomite recrystallization. D2 is the dolomite type with the best reservoir performance in the Xixiangchi Formation, mainly developed in high-energy sedimentary facies. Early seepage-reflux dolomitization and atmospheric freshwater dissolution are crucial for reservoir development. Burial dolomitization promotes secondary pore development in D3 and D4, increasing porosity, but recrystallization blurs crystal grains and reduces porosity. Evaporation dolomitization creates dense dolomite, making D1 have the poorest porosity. In conclusion, reservoir quality primarily depends on particle shoal development through paleo-uplift and fault-controlled mechanisms, with diagenetic processes (dolomitization, dissolution, fracturing) crucially enhancing porosity preservation and formation.

KEYWORDS

reservoir characteristics, geochemical constraints, diagenesis, middle-upper Cambrian, Xixiangchi formation, Sichuan Basin

1 Introduction

As an important carrier of global oil and gas resources, carbonate reservoirs have complex diagenetic evolution processes, strong heterogeneity, and multi-scale pore structure characteristics, which have always been research hotspots in the fields of petroleum geology and development. Carbonate rocks also make a significant contribution to the global oil and gas production. For example, the Middle East, as a major global oil-producing region, has a large proportion of carbonate rock oil and gas. In addition, there are oil and gas fields such as the Cabin Creek carbonate oil and gas field in the Upper Devonian of Alberta, Canada, the Puckett dolomite oil and gas field in the Lower Ordovician of Texas, the United States, and the carbonate gas field in the Carboniferous of Uktur, Russia (Khaled et al., 2020; Husinec and Jelaska, 2006; Sun, 1995; Friedman and Sun, 1994; Roehl and Choquette, 1985). Dolomite reservoirs, which make up over 50% of global hydrocarbon reserves and production (Luo et al., 2008; Ma, 2011), play a crucial role in carbonate reservoir systems. Therefore, understanding dolomitization mechanisms is essential for studying carbonate reservoirs (Tucker and Wright, 1990; Warren, 2000; Machel, 2004; Gomez-Rivas et al., 2014; Liu et al., 2020). Dolomitization impacts reservoir quality through various genetic models, including: 1) evaporation-reflux (Warren, 2000; Machel, 2004; Ryan et al., 2020), 2) mixed-water (Badiozamani, 1973; Barnaby and Read, 1992; Luczaj, 2006), 3) seawater (Land, 1985; Manche and Kaczmarek, 2019), 4) burial, and 5) hydrothermal processes (Davies and Smith Jr, 2006; Morrow, 2014; Jiu et al., 2020). This provides us with a reference and guidance for further studying the impact of the dolomite model on reservoir development.Each model has distinct geological constraints, diagenetic fluids, and impacts on pore architecture and reservoir performance. Resolving regional dolomitization mechanisms requires a systematic analysis of fluid characteristics and diagenetic environments can be elucidated through geochemical proxies (e.g., $\delta^{13}C$, $\delta^{18}O$, and rare earth elements), which reveal fluid sources and diagenetic evolution (Tucker and Wright, 1990; Warren, 2000; Machel, 2004; Özyurt et al., 2019).

Current research on the Xixiangchi Formation in the Sichuan Basin focuses on central and southeastern regions, addressing sequence stratigraphy (Jia et al., 2017; Li W. et al., 2019; Jing et al., 2016), lithofacies paleogeography (Gu et al., 2020; Li and He, 2014; Wen et al., 2022), reservoir controls (Li et al., 2016; Jiang et al., 2015; Deng et al., 2022), and dolomite genesis. While multiple dolomitization models (penecontemporaneous, mixed-water, burial) have been proposed (Lei et al., 2016; Peng et al., 2018; Jiang et al., 2016a; Ren et al., 2022). Additionally, previous studies on the dolomite reservoirs of the Xixiangchi Formation have mostly focused on single regions or single factors (such as sedimentary facies or diagenesis), lacking cross-regional systematic comparative studies on the differences in dolomite reservoirs between the central and southern Sichuan Basin. The impacts of tectonic-sedimentary-diagenetic processes during the Xixiangchi Formation period on the central and southern Sichuan regions have not been clarified, and the developmental characteristics and formation mechanisms of dolomite reservoirs remain poorly understood. Therefore, studying the differences in dolomite reservoirs between the central and southern Sichuan Basin not only represents new accumulative research on the Xixiangchi Formation dolomite reservoirs within the basin but also holds significant indicative value for evaluating the tectonic environment, fluid properties, and oil-gas exploration potential of the Xixiangchi Formation in the Sichuan Basin. This study integrates regional sediment-tectonic frameworks, petrographic analysis, and geochemical data ($\delta^{13}C$, $\delta^{18}O$, rare earth elements) to investigate dolomitization processes and their reservoir-enhancing effects in central-southern Sichuan Basin, providing insights for sustainable hydrocarbon exploration.

2 Geological setting

The Sichuan Basin, which spans central-eastern Sichuan Province and most of Chongqing Municipality, constitutes a large, long-evolved superimposed hydrocarbon-bearing basin in western China (Zhao et al., 2015). Tectonically positioned northwest of the Yangtze paraplatform, this first-order structural unit forms a rhombic-shaped basin (area: ~260,000 km^2) shaped by NE- and NW-trending deep faults within the Yangtze platform. The basin comprises six structural domains: 1) western Sichuan low-gentle fault-fold belt, 2) northern Sichuan gentle fault-fold belt, 3) southwestern Sichuan low-gentle fault-fold belt, 4) central Sichuan gentle fault-fold belt, 5) southern Sichuan low-steep fault-fold belt, and 6) eastern Sichuan high-steep fault-fold belt.

Our study area is located in the southern basin sector, borderd by Shizhu (east), Gulin-Junlian (south), Leshan (west), and Dazhou (north), encompassing the southern Sichuan low-steep and southwestern Sichuan low-gentle fault-fold belts (Figure 1). During the deposition of the Xixiangchi Formation deposition, the Upper Yangtze platform developed an extensive carbonate rimmed platform system, recording a major transgressive-regressive cycle with northwestward stratigraphic thinning (Wen et al., 2022). Lateral facies transitions progress westto east, startingfrom mixed tidal flats and moving through restricted to open platform facies, transitioning further eastward to platform-margin and slope-basin facies in western Hunan-Hubei. Deposition in the southern Southern basin primarily features restricted platform sequences, which are futher subdivided into grain bank and lagoon subfacies. The Xixiangchi Formation maintains conformable contacts with both the overlying Tongzi (488.3 - 471.8 Ma) and underlying Gaotai formations (509 - 485.4 Ma) (Lin et al., 2017), exhibiting well-developed grainstone and crystalline dolostones, with argillaceous dolostones predominating in the upper and lower sections.

3 Samples and methods

Core samples were obtained from five wells in the central Sichuan Basin (GT2, MX39, H12, AP1, LG1) and three locations in southern Sichuan Basin (SH and HT outcrops, WH1 well). A total of 181 samples with visible porosity were selected for epoxy-impregnated microphotographs to characterize pore networks. Routine microphotographs were prepared from 201 samples, with mirror-polished thick sections created for dolomite micro-drilling to avoid contamination by late-stage vein-filling minerals. All microphotographs underwent alizarin red-S staining (Dickson, 1966) for carbonate mineral discrimination. Cathodoluminescence (CL) microscopy was conducted on 150 representative dolomite samples using a CL8200 MK5 system (Chengdu University of Technology) at 15 kV accelerating voltage and 330 μA beam current. Scanning electron microscopy (SEM) analysis utilized a Quanta 250 FEG instrument (State Key Laboratory of Oil and Gas Reservoir Geology and Development, Chengdu University of Technology) to examine 22 dolomite specimens (1 cm^3 cubes) at 5 kV acceleration voltage to observe the morphology of dolomite crystals and the microscopic pore structure, etc. For the purpose of geochemical analysis, the following samples were selected respectively: micritic (n = 14), fabric-retentive (n = 15), very fine grained crystalline (n = 18), and fine-medium grained crystalline (n = 16) dolomite textures. Micro-drilled powders (<200 mesh) were extracted from homogeneous zones avoiding veins and diagenetically altered areas.

3.1 Analysis of major and trace elements

The analysis of trace elements in whole rock was conducted at the Experimental Center of the School of Earth Sciences, Yangtze University. The content of major elements was determined using an Inductively Coupled Plasma Optical Emission Spectrometer (ICP-OES) according to GB/T 14,506.31-2019. The procedure is as follows: approximately 30 mg of dolomite powder sample was placed in a 15 mL centrifuge tube, and 5 mL of 0.5 mol/L acetic acid was added to dissolve the powder. The centrifuge tube was then placed in an ultrasonic bath for 30 min, followed by centrifugation at 3000 rpm for 10 min. The supernatant was collected for elemental composition determination using an Inductively Coupled Plasma Mass Spectrometer (ICP-MS). The relative error of the detection results was less than 3%; the content of trace elements was analyzed using the Agilent 7700e ICP-MS.

3.2 Carbon and oxygen isotope analysis

The carbon and oxygen isotope analysis was conducted using the whole-rock McCrea (1950) phosphoric acid method, with sample testing completed at the Geochemistry Laboratory of Yangtze University. The carbon and oxygen isotope values of the samples were determined using standard analytical methods. Under vacuum conditions at 25°C, CO_2 was generated by reacting with 100% phosphoric acid for 24 h using the inverted Y-tube technique. The produced CO_2 gas was collected and sent to a Finnigan MAT 252 gas mass spectrometer for the detection of inorganic carbon and oxygen isotope compositions. The carbon and oxygen isotopes were calibrated using stable isotope reference materials (IAEA-CO-8), with the PDB (Pee Dee Belemnite) international standard as the reference. The analytical deviations were: $\delta^{13}C < \pm 0.2‰$, $\delta^{18}O < \pm 0.3‰$.

3.3 Strontium isotope analysis

Strontium isotope analysis was carried out at the State Key Laboratory of Oil and Gas Reservoir Geology and Development Engineering, Chengdu University of Technology. The analytical testing process is as follows: Weigh 50 mg of powder sample below 200 mesh, add 5 mL of 1 M acetic acid to dissolve the sample (for 2 h). After centrifugation, take the supernatant and evaporate it to dryness. Then add 1 mL of concentrated nitric acid to dissolve the residue, and repeat this operation twice to remove acetic acid. After evaporating to dryness again, add 5 mL of 1 M nitric acid to dissolve the sample and form the solution to be tested. The instrument used for determination is a Neptune Plus MC - ICP - MS. The test precision for the NBS SRM 987 standard sample is 0.710289 ± 0.000015 (2σ, n = 14). The analysis process was conducted in accordance with the National Standard of the People's Republic of China*Method for Determination of Strontium Isotopes in Rocks*(GB/T 17,672 - 1999) to ensure the standardization and scientificity of the analysis.

4 Results

4.1 Reservoir characteristics

4.1.1 Reservoir rock types

Overall, the Cambrian Xixiangchi Formation reservoir rocks in the Sichuan Basin mainly consist of four types: microcrystalline dolomite (D1), fabric-retentive dolomite (D2), very finely to finely crystalline dolomite (D3), and finely to medium crystalline dolomite (D4).

D1 exhibits thin to medium-thick layered structures with dense textures (Figures 2a,b). Microscopic observations reveal laminated structures formed by localized enrichment of muddy and silty

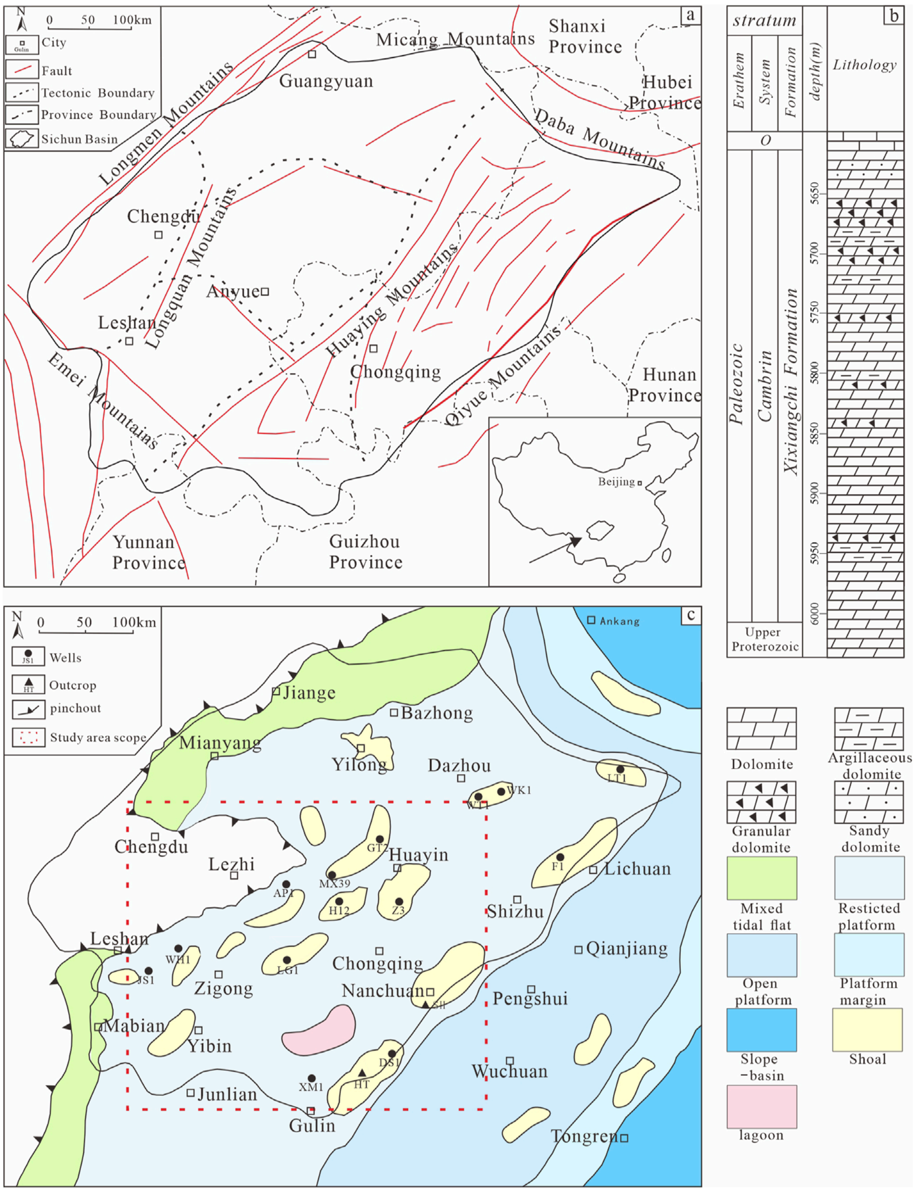

FIGURE 1
(a) Map showing the location and general structural units of Sichuan Basin (were modified after Su et al., 2022; Liang et al., 2022). **(b)** General lithological column showing the Cambrian depositional successions in the Sichuan Basin (were modified after Wen et al., 2022). **(c)** The paleogeographic map shows the sedimentary framework of the Sichuan Basin during the Xixiangchi Formation (were modified after Zhao et al., 2015; Deng et al., 2022).

materials (Figure 2a), suggesting deposition in relatively low-energy environments. Scanning electron microscopy (SEM) shows planar-subhedral to euhedral dolomite crystal faces with compact microstructures (Figure 2b).

D2, one of the primary reservoir lithologies in the Xixiangchi Formation, predominantly develops in granular shoals. It features thin single-layer thickness, with intergranular spaces often filled by fine-silty dolomite, and contains fractures and intergranular pores. Common grains include sand-sized clasts (0.16–0.4 mm, irregular morphology; Figures 2c,d) and ooids, with grain content ranging 50%–97%. Among them, dolarenite and oolitic dolomite are subtypes of D2. Enhanced cathodoluminescence intensity around pore edges indicates atmospheric freshwater dissolution (Figure 2e). Recrystallization modification has significantly altered internal grain structures in some areas (Figures 2f,g).

D3 appears gray and comprises silty to very fine-crystalline dolomite (85% silty-fine crystals, 15% micritic-dolomicrite). Crystal sizes range 0.01–0.1 mm (subhedral to anhedral), often containing microfractures filled by dolomite, bitumen, or minor calcite (Figures 2h,i). Studies indicate that bitumen-filled intercrystalline dissolution pores and stylolite-associated dissolution features reflect acidic fluid dissolution (Hu et al., 2009).

D4 consists of euhedral to subhedral fine-crystalline dolomite (0.1–0.25 mm crystals), likely products of shallow burial dolomitization. Characteristic “foggy-core bright-edge” textures (Figure 2j) and ghost granular structures (Figure 2k) suggest origins

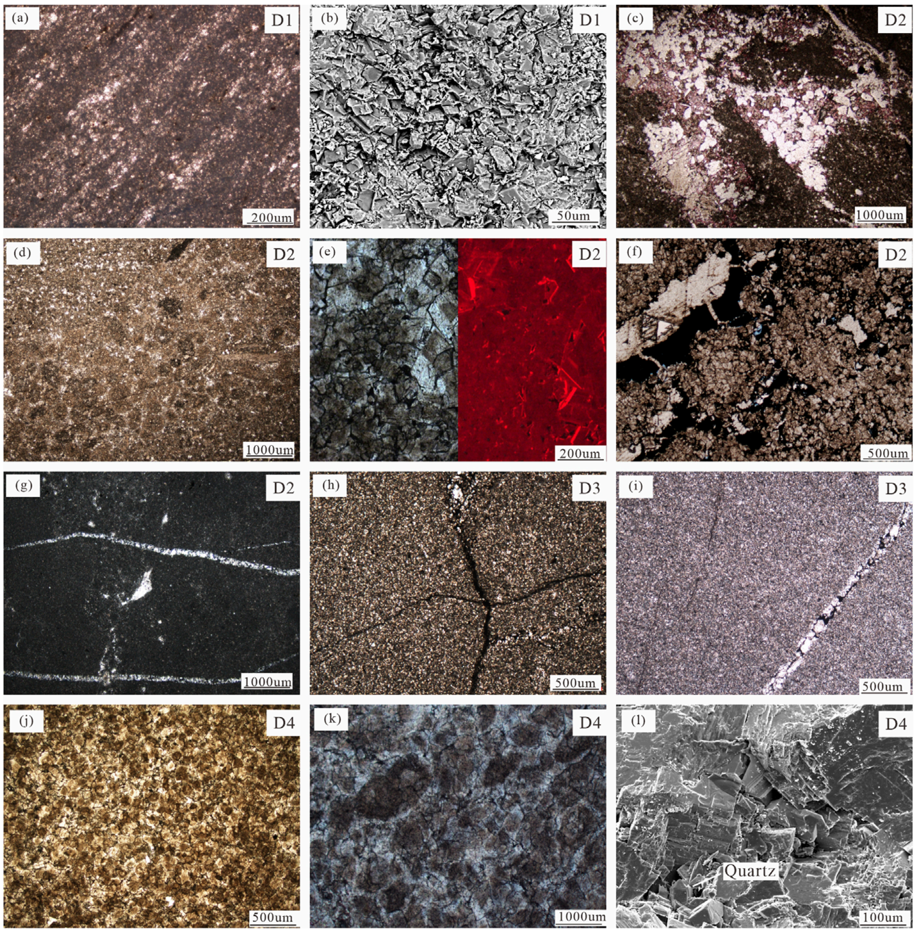

FIGURE 2
Microphotographs showing, **(a)** D1, exhibiting laminated structures, SH35-2, under plane polarized light; **(b)** residual particles with crystals more densely cemented, SEM, SH17-1; **(c)** D2, locally filled saddle-shaped dolomite, HT11-4, under plane polarized light; **(d)** D2, locally banded accumulation of fine crystalline dolomite, WH1, 2261.59 m, under plane polarized light; **(e)** D2, under plane polarized light and CL, SH19-2; **(f)** D2, fracture-filling asphalt, GT2 well, 5320.17 m, under plane polarized light; **(g)** D2, medium crystalline dolomite filling in solution pores, SH3-1, under plane polarized light; **(h)** D3, GT2 well, 5317.7 m, under plane polarized light; **(i)** D3, weathering joint filled with calcite, SH29-1,under plane polarized light; **(j)** D4, partially visible misty bright edge structure, SH50-2, under plane polarized light; **(k)** D4, primarily grain structure with cloudy core and bright rim, SH5-1, under plane polarized light; **(l)** D4, pore-filling quartz, SEM, SH45-1.

from further recrystallization of residual granular dolostone, with well-developed intercrystalline and dissolution pores. SEM observations reveal quartz infillings (Figure 2l).

4.1.2 Reservoir pore types

The dolomite reservoir spaces in the Xixiangchi Formation are broadly classified into primary, secondary (dissolution), and fracture porosity. Primary porosity types include intergranular pores (0.08–0.2 mm irregular polygons in dolarenite; Figure 3a) and intercrystalline pores (0.001–0.2 mm regular geometries predominantly in very fine grained crystalline dolomites; Figures 3b,c). Secondary dissolution porosity comprises three subtypes: (1) intergranular dissolution pores formed through meteoric freshwater leaching, often partially occluded by quartz and calcite cement in dolarenite and oolitic dolomite (Figure 3d); (2) intercrystalline dissolution pores with irregular polygonal morphologies and corroded edges (Figure 3e); and (3) large-scale dissolution vugs (>2 mm diameter) exhibit two genetic patterns - expanded intergranular dissolution voids forming honeycomb structures in fabric retentive dolomites (Figures 3f,h) and altered crystalline dolomite pores partially filled with bitumen and dolomite (Figure 3g). Fracture systems consist of structural fractures (tectonically induced, dolomite/calcite-filled; Figure 3i), dissolution-enlarged fractures with variable apertures (Figure 3j), or anhydrite-cemented examples in Figure 3l, and stylolites containing bitumen impregnations (Figure 3k) formed through pressure dissolution. These fracture networks facilitate fluid migration and enhance diagenetic alteration processes (Zheng, 2019), with dissolution features showing spatial association with acidic fluids (organic acids/CO_2) during burial diagenesis and meteoric water infiltration (Jiang et al., 2016b).

4.1.3 Analysis of reservoir physical properties

The Cambrian Xixiangchi Formation dolomite reservoirs in the study area exhibit porosity values predominantly ranging from 0.7% to 6.8%, with 93.4% of samples below 2.0% porosity

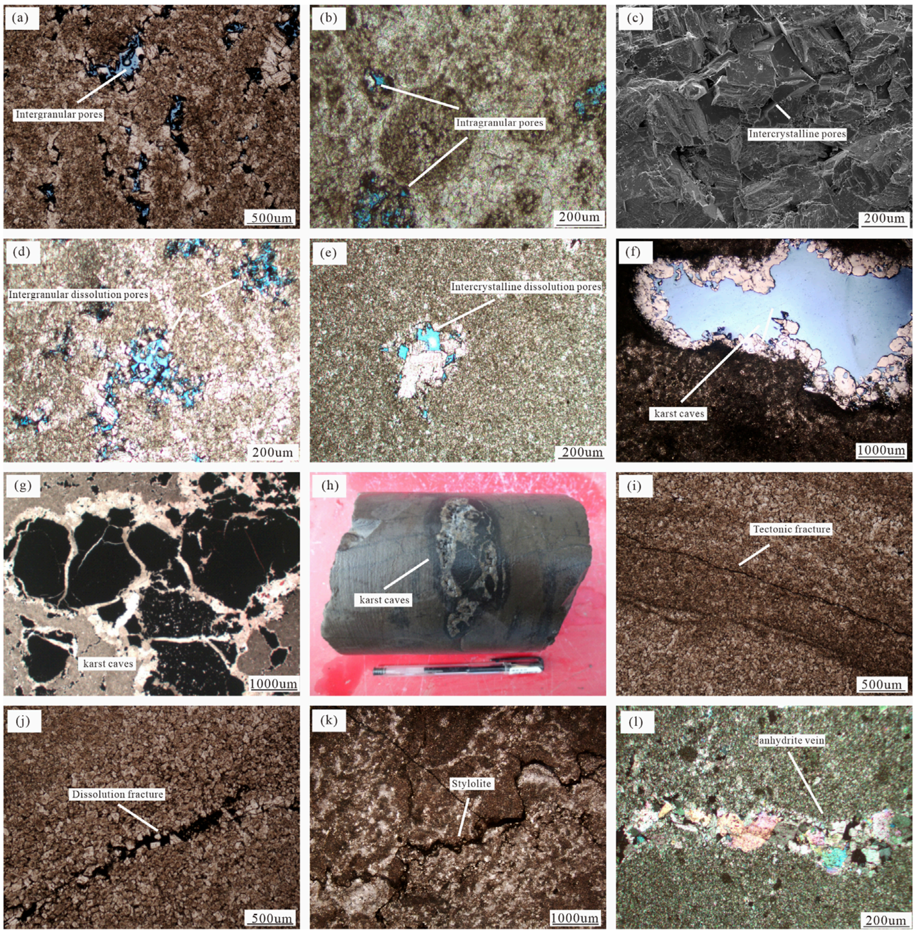

FIGURE 3
Microphotographs showing, **(a)** D2, intergranular pores completely filled with asphalt, LG1 Well, 4416.8 m, under plane polarized light; **(b)** D4, crystal intergranular pores, LG1 Well, 4415.2 m, under plane polarized light; **(c)** subhedral dolomite, showing crystal intergranular pores, SEM, SH45-1; **(d)** D2, intergranular dissolution pores, SH8-1, under plane polarized light; **(e)** D3, crystal dissolution pores, Sanhui profile, SH9-1, under plane polarized light; **(f)** D4, cave wall filled with quartz and fine to medium crystalline dolomite, SH31-2, under plane polarized light; **(g)** D2, caves filled with asphalt and dolomite cement, MX39 Well, 4682.49 m, under plane polarized light; **(h)** gray to dark gray D2, caves filled with collapse breccia, GT2 Well, 5355.45–5355.57 m; **(i)** D3, developed structural fractures, LG1 Well, 4415.2 m, under plane polarized light; **(j)** D4, dolomite filling dissolution fractures, LG1 Well, 4419 m, under plane polarized light; **(k)** D2, seams filled with organic matter, SH22-1, under plane polarized light; **(l)** D1, hard gypsum vein cementation, HT42-1, orthogonal polarized light.

(average 1.1%). Permeability measurements show 77.8% of samples below $0.01 \times 10^{-3}\ \mu m^2$, while only 0.7% exceed $10 \times 10^{-3}\ \mu m^2$ (average 1.0%) (Figure 4). These parameters collectively define the reservoirs as low-porosity, low-permeability systems. Porosity-permeability correlation analysis reveals poor interdependence ($R^2 = 0.31$), suggesting fracture-dominated fluid flow pathways rather than matrix-controlled permeability. An exception occurs in Well GT2 of the central Sichuan Basin, which demonstrates an improved porosity-permeability correlation indicative of matrix-supported porous reservoirs.

Porosity distribution across six sampled locations (Well GT2, H12, AP1, WH1, HT and SH profiles) shows systematic spatial variation (Figure 5). Wells in the central Sichuan Basin wells (GT2, H12, AP1) yield higher average porosities (1.8%–2.82%) compared to their southern counterparts (WH1: 1.28%; HT: 1.53%; SH: 1.29%). Measured values range from 0.44% (H12) to 4.05% (GT2), with specific distributions as follows: GT2 (n = 10, 0.8%–4.05%, avg 2.82%), H12 (n = 12, 0.44%–3.21%, avg 1.47%), AP1 (n = 13, 0.83%–2.72%, avg 1.42%), WH1 (n = 17, 0.45%–3.2%, avg 1.28%), HT (n = 14, 0.60%–2.22%, avg 1.53%), and SH (n = 11, 0.69%–2.19%, avg 1.53%) (Figure 6). This heterogeneous distribution, featuring localized high-porosity anomalies within generally tight matrices, reflects complex controls from depositional facies, diagenetic modification, and structural fracturing.

4.2 Geochemical characteristics

4.2.1 Carbon and oxygen isotopes

Stable isotope analyses reveal distinct signatures across different types of dolomite. D1 (n = 14) exhibits $\delta^{13}C_{VPDB}$ values of −2.2‰ to +0.59‰ (mean −1.39‰ ± 0.67‰) paired with $\delta^{18}O_{VPDB}$ values of −10.09‰ to −6.42‰ (mean −8.42‰ ± 1.07‰). D2 (n = 15) show $\delta^{13}C$ values of −2.79‰ to +0.27‰ (mean −1.26‰ ± 0.6‰) and $\delta^{18}O$

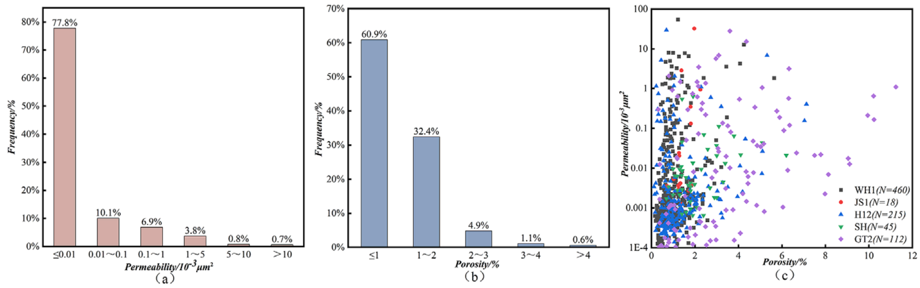

FIGURE 4
Characteristics of porosity and permeability of dolomite of Xixiangchi Formation in southern Sichuan Basin. **(a)** Frequency distribution map of porosity of dolomite; **(b)** Frequency distribution map of permeability of dolomite; **(c)** Porosity and Permeability Cross-plot of Dolomite.

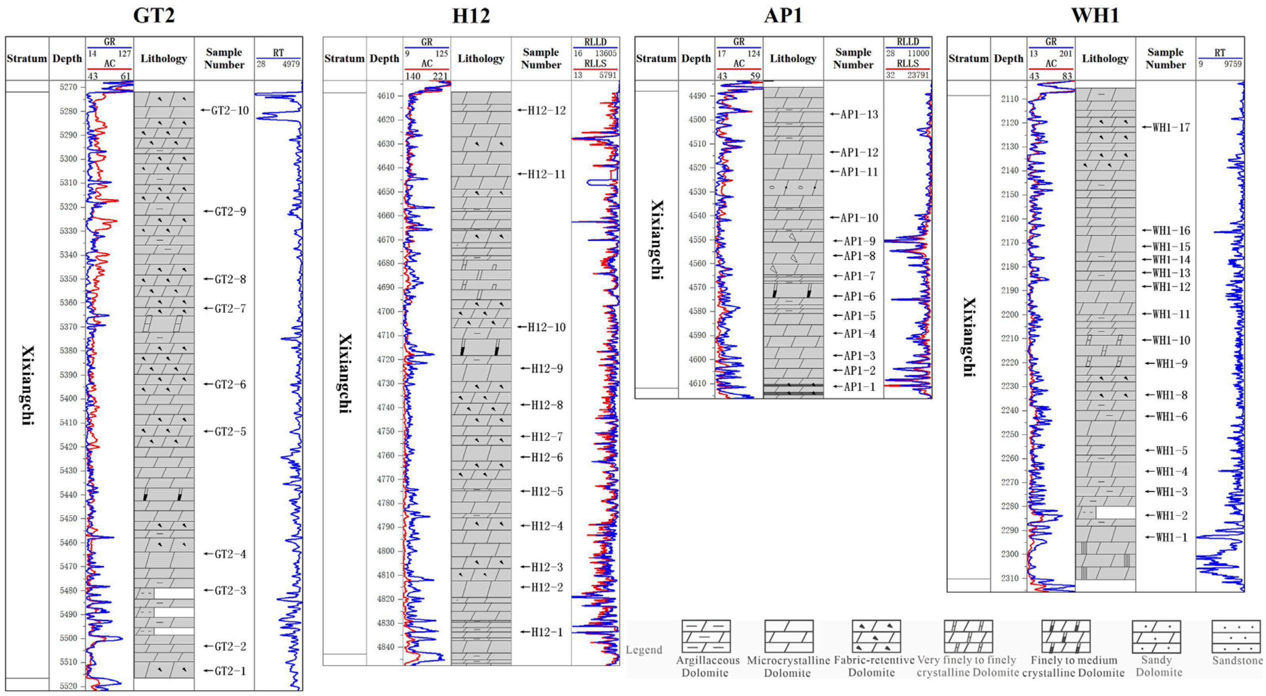

FIGURE 5
Integrated well columnar profiles and sampling positions of the Xiangxichi Formation in the Sichuan Basin.

values of −10.67‰ to −6.62‰ (mean −8.27‰ ± 1.28‰). D3 (n = 18) display $\delta^{13}C$ values of −2.89‰ to −0.14‰ (mean −1.48‰ ± 0.74‰) and $\delta^{18}O$ values of −11.05‰ to −6.11‰ (mean −8.53‰ ± 1.37‰). D4 (n = 16) demonstrate $\delta^{13}C$ values of −2.28‰ to −0.13‰ (mean −1.23‰ ± 0.71‰) with $\delta^{18}O$ values of −10.65‰ to −6.98‰ (mean −8.62‰ ± 1.18‰) (Table 1; Figure 7).

4.2.2 Strontium isotopes

Initial $^{87}Sr/^{86}Sr$ measurements range form 0.70788–0.70972 (mean 0.70870). Post-quality control exclusion of magnetically suspect data points,the $^{87}Sr/^{86}Sr$ values range form 0.70934–0.71074 (mean 0.70969, n = 21). Stratigraphic variations show D1: 0.70945–0.71027 (0.70973 ± 0.00031, n = 4); D2: 0.70934–0.71074 (0.70974 ± 0.00042, n = 8); D3: 0.70937–0.70967 (0.70953 ± 0.00011, n = 5); D4: 0.70955–0.70990 (0.70974 ± 0.00015, n = 4). Although the $^{87}Sr/^{86}Sr$ ratios show limited variation (Δ = 0.00041), a subtle decreasing trend emerges from D1 to D4 (Figure 8).

4.2.3 Major and trace elements

4.2.3.1 Sc-Th-U

4.2.3.1.1 Central Sichuan basin Regarding the Sc content, the Sr content distribution range of D1 is0.8–1.6 ppm (1.2 ± 0.3 ppm, n = 3); that of D2 is 0.4–3.6 ppm (1.2 ± 1.0 ppm, n = 8); that of D3 is 0.5–2.8 ppm (1.1 ± 0.8 ppm, n = 6); and that of D4 is 0.5–3.7 ppm (1.4 ± 1.2 ppm, n = 8). Regarding the Th content, the Th content distribution range of D1 is 0.3–1.3 ppm (0.8 ± 0.4 ppm, n = 3); that of D2 is 0.3–2.6 ppm (1.1 ± 0.9 ppm, n = 8); that of D3 is 0.4–2.3 ppm (0.9 ± 0.7 ppm, n = 6); and that of D4 is 0.3–2.3 ppm (1.0 ± 0.8 ppm,

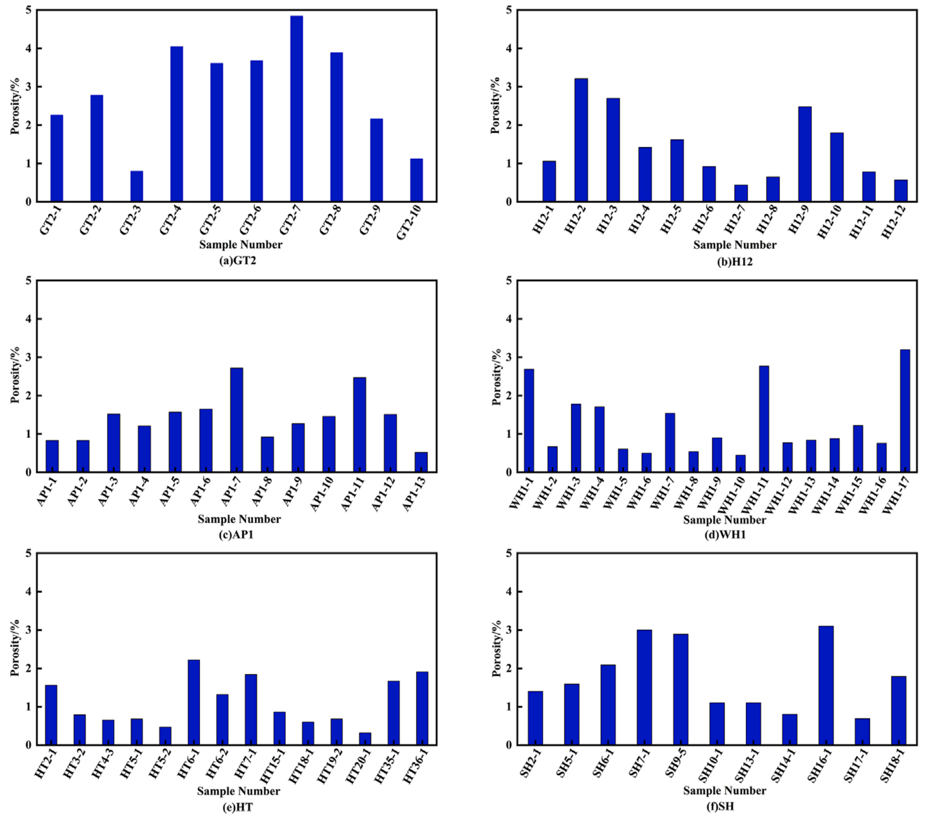

FIGURE 6
Porosity distribution of different outcrop and core samples of the Xixiangchi Formation **(a)** GT2, **(b)** H12, **(c)** AP1, **(d)** WH1, **(e)** HT, **(f)** SH.

n = 8). Regarding the U content, the U content distribution range of D1 is 0.3–0.8 ppm (0.5 ± 0.2 ppm, n = 3); that of D2 is 0.2–1.2 ppm (0.6 ± 0.4 ppm, n = 8); that of D3 is 0.4–2.1 ppm (0.7 ± 0.6 ppm, n = 6); and that of D4 is 0.3–0.9 ppm (0.5 ± 0.2 ppm, n = 8) (Table 1).

4.2.3.1.2 Southern Sichuan Basin Regarding the Sc content, the Sr content distribution range of D1 is 0.5–1.0 ppm (0.7 ± 0.2 ppm, n = 4); that of D2 is 0.2–0.4 ppm (0.3 ± 0.1 ppm, n = 4); that of D3 is 0.2–0.6 ppm (0.4 ± 0.2 ppm, n = 3); and that of D4 is 0.4–1.2 ppm (0.7 ± 0.3 ppm, n = 4). Regarding the Th content, the Th content distribution range of D1 is 0.2–0.9 ppm (0.6 ± 0.3 ppm, n = 4); that of D2 is 0.1–0.3 ppm (0.2 ± 0.1 ppm, n = 4); that of D3 is 0.1–0.6 ppm (0.3 ± 0.4 ppm, n = 3); and that of D4 is 0.3–0.5 ppm (0.4 ± 0.1 ppm, n = 4). Regarding the U content, the U content distribution range of D1 is 0.4–0.6 ppm (0.4 ± 0.4 ppm, n = 4); that of D2 is 0.1–0.2 ppm (0.3 ± 0.1 ppm, n = 4); that of D3 is 0.1–0.4 ppm (0.2 ± 0.1 ppm, n = 3); and that of D4 is 0.1–0.2 ppm (0.2 ± 0.1 ppm, n = 4) (Table 1).

4.2.3.2 Fe-Mn-Sr

Fe and Mn are sensitive to redox environments, and the ionic radii of their lower valence states are close to those of Ca^{2+} and Mg^{2+}. Therefore, the more reducing the conditions, the more favorable it is for Fe^{2+} and Mn^{2+} to enter the dolomite lattice and substitute for Ca^{2+} and Mg^{2+}.

4.2.3.2.1 Central Sichuan basin The Fe content from D1 to D4: D1 (1643.7–6840.5 ppm, 3818.9 ± 2204.4 ppm, n = 3), D2 (1400.8–6860.8 ppm, 3042.6 ± 1963.0 ppm, n = 8), D3 (1398.9–9332.6 ppm, 2944.6 ± 2821.5 ppm, n = 6), and D4 (1217.0–5958.6 ppm, 3315.9 ± 2518.9 ppm, n = 8). The Mn content from D1 to D4: D1 (154.9–193.6 ppm, 175.6 ± 16.0 ppm, n = 3), D2 (123.9–333.0 ppm, 203.2 ± 67.1 ppm, n = 8), D3 (147. 2–353.8 ppm, 203.4 ± 70.2 ppm, n = 6), and D4 (158.4–213.5 ppm, 179.6 ± 17.0 ppm, n = 8). Regarding the Sr content, the distribution range of Sr content in D1 is 128.4–141.7 ppm (135.5 ± 5.5 ppm, n = 3); in D2, it is 101.5–249.9 ppm (135.2 ± 47.1 ppm, n = 8); in D3, it is 111.5–193.6 ppm (134.7 ± 27.1 ppm, n = 6); and in D4, it is 96.7–121.1 ppm (107.0 ± 8.5 ppm, n = 8) (Table 1).

4.2.3.2.2 Southern Sichuan Basin The Fe content from D1 to D4: D1 (1091.1–5036.0 ppm, 2796.0 ± 1519.9 ppm, n = 4), D2 (832.3–1349.9 ppm, 1045.7 ± 196.3 ppm, n = 4), D3 (713.4–2049.4 ppm, 1550.4 ± 295.5 ppm, n = 3), and D4 (1126.1–4056.7 ppm, 2098.3 ± 1153.9 ppm, n = 4). The Mn content from D1 to D4: D1 (100.7–139.4 ppm, 1118.1 ± 14.9 ppm, n = 4), D2 (54.2–170.4 ppm, 104.6 ± 49.0 ppm, n = 4), D3 (131.7–209.1 ppm, 170.4 ± 31.7 ppm, n = 3), and D4 (100.7–154.9 ppm, 125.9 ± 22.2 ppm, n = 4). Regarding the Sr content, the distribution range of Sr content in D1 is 49.4–66.7 ppm (59.1 ± 6.3 ppm, n = 4); in D2, it is 32.6–99.0 ppm (66.0 ± 29 ppm, n = 4); in D3, it is 31.4–132.1 ppm

TABLE 1 Summary of statistics of $\delta^{13}C$, $\delta^{18}O$, major and trace element of the investigated Xixiangchi Formation carbonates in eastern Sichuan Basin. The $\delta^{13}C$ and $\delta^{18}O$ values are in ‰VPDB and the elemental concentrations are in ppm.

Phase	Statistics	$\delta^{13}C$	$\delta^{18}O$	$^{87}Sr/^{86}Sr$	TiO_2	Fe_2O_3	MnO	SiO_2	Fe	Mn	Sr	Sc	Th	U	Mn/Sr
D1	n	14	14	4	8	8	8	8	7	7	7	7	7	7	7
	mean	−1.39	−8.42	0.70973	0.08	0.57	0.022	16.01	1685.25	142.72	91.85	0.95	0.67	0.45	1.72
	S.D.	0.67	0.98	0.00031	0.05	0.26	0.012	13.12	271.67	32.29	38.25	0.35	0.35	0.18	0.51
	Max	0.59	−6.42	0.70945	0.18	0.93	0.018	35.98	2035.95	193.62	141.68	1.61	1.27	0.77	2.82
	Min	−2.2	−9.63	0.71027	0.01	0.16	0.005	0.79	1091.12	108.43	49.36	0.49	0.23	0.2	1.09
D2	n	15	15	8	9	9	9	9	12	12	12	12	12	12	12
	mean	−1.26	−8.27	0.70965	0.04	0.33	0.019	6.44	1793.64	170.29	112.14	0.92	0.8	0.43	4.613
	S.D.	0.67	1.28	0.00047	0.04	0.24	0.008	6.93	757.69	77.09	53.11	0.96	0.87	0.36	0.62
	Max	0.27	−6.62	0.71074	0.12	0.81	0.032	23.3	3301.34	333.02	249.84	3.60	2.16	1.19	2.21
	Min	−2.79	−10.67	0.70924	0.01	0.12	0.001	0.55	832.33	54.21	32.59	0.18	0.12	0.11	0.6
D3	n	18	18	5	7	7	7	7	9	9	9	9	9	9	9
	mean	−1.48	−8.54	0.70953	0.05	0.4	0.021	5.87	1968.74	192.39	117.17	0.83	0.66	0.56	1.95
	S.D.	0.74	1.36	0.00011	0.04	0.38	0.004	2.19	330.99	62.12	40.85	0.71	0.61	0.56	1.05
	Max	−0.14	−6.11	0.70967	0.13	1.32	0.028	10.02	2713.43	353.76	193.6	2.82	2.26	2.07	4.19
	Min	−2.89	−11.05	0.70937	0.02	0.2	0.016	2.7	1598.87	131.66	31.41	0.17	0.13	0.09	0.96
D4	n	16	16	4	7	7	7	7	12	12	12	12	12	12	12
	mean	−1.22	−8.63	0.70939	0.02	0.25	0.021	4.38	2618.36	161.69	96.49	1.19	0.82	0.4	1.87
	S.D.	0.72	1.19	0.00017	0.01	0.05	0.004	2.85	987.42	31.61	30.78	1.03	0.71	0.25	0.63
	Max	−0.13	−6.98	0.70963	0.03	0.29	0.027	10.16	5741.8	190.87	151.25	3.73	2.32	0.87	3.13
	Min	−2.28	−10.31	0.7092	0.02	0.17	0.015	1.17	1933.85	100.68	34.70	0.35	0.27	0.08	1.35

Phase		La	Ce	Pr	Eu	Gd	Tb	Dy	Ho	Er	Tm	Yb	Lu	ΣREE	(Nd/Yb)sn	δCe	δEu	δPr
D1	n	8	8	8	8	8	8	8	8	8	8	8	8	8	8	8	8	8
	mean	2.64	5.50	0.69	0.09	0.51	0.11	0.52	0.10	0.28	0.04	0.28	0.04	14.09	0.84	0.91	0.73	1.08
	S.D.	1.22	2.58	0.31	0.05	0.24	0.04	0.25	0.05	0.12	0.02	0.14	0.02	6.18	0.34	0.07	0.21	0.03
	Max	4.49	9.53	1.18	0.11	0.75	0.12	0.75	0.15	0.36	0.05	0.29	0.04	23.01	1.22	0.98	1.12	1.13
	Min	0.91	1.91	0.23	0.02	0.13	0.12	0.12	0.02	0.16	0.01	0.15	0.01	4.75	0.38	0.73	0.50	1.07
D2	n	9	9	9	9	9	9	9	9	9	9	9	9	9	9	9	9	9
	mean	2.43	4.65	0.53	0.07	0.36	0.06	0.33	0.06	0.18	0.03	0.17	0.03	11.17	1.05	0.92	0.83	1.07
	S.D.	1.22	2.75	0.31	0.05	0.24	0.04	0.24	0.05	0.13	0.02	0.14	0.02	6.61	0.29	0.06	0.17	0.06
	Max	4.55	9.61	1.15	0.17	0.80	0.13	0.76	0.15	0.42	0.07	0.33	0.07	23.21	1.51	1.02	1.20	1.22
	Min	1.15	2.29	0.27	0.03	0.18	0.03	0.15	0.03	0.07	0.01	0.06	0.01	5.48	0.53	0.84	0.62	1.01

(Continued on the following page)

TABLE 1 (*Continued*) Summary of statistics of $\delta^{13}C$, $\delta^{18}O$, major and trace element of the investigated Xixiangchi Formation carbonates in eastern Sichuan Basin. The $\delta^{13}C$ and $\delta^{18}O$ values are in ‰VPDB and the elemental concentrations are in ppm.

Phase		La	Ce	Pr	Eu	Gd	Tb	Dy	Ho	Er	Tm	Yb	Lu	ΣREE	(Nd/Yb)sn	δCe	δEu	δPr
D3	n	7	7	7	7	7	7	7	7	7	7	7	7	7	7	7	7	7
	mean	2.30	4.43	0.52	0.09	0.39	0.06	0.37	0.07	0.20	0.03	0.23	0.03	11.09	0.87	0.93	0.91	1.05
	S.D.	1.14	1.99	0.18	0.05	0.16	0.03	0.17	0.03	0.10	0.02	0.14	0.02	4.79	0.31	0.05	0.12	0.06
	Max	4.912	8.767	0.832	0.177	0.671	0.113	0.663	0.131	0.387	0.066	0.491	0.065	21.05	1.28	0.99	1.14	1.16
	Min	1.25	2.13	0.25	0.03	0.16	0.02	0.14	0.03	0.07	0.01	0.06	0.01	5.23	0.53	0.88	0.77	0.93
D4	n	7	7	7	7	7	7	7	7	7	7	7	7	7	7	7	7	7
	mean	2.19	4.02	0.47	0.06	0.31	0.05	0.28	0.06	0.14	0.02	0.14	0.02	9.81	1.13	0.91	0.92	1.06
	S.D.	0.44	0.82	0.12	0.01	0.08	0.01	0.09	0.02	0.04	0.01	0.05	0.01	2.10	0.26	0.06	0.09	0.06
	Max	2.95	5.19	0.64	0.08	0.44	0.07	0.44	0.09	0.22	0.03	0.20	0.03	12.43	1.43	0.96	1.05	1.19
	Min	1.71	2.85	0.32	0.05	0.19	0.03	0.16	0.03	0.08	0.01	0.07	0.01	6.88	0.59	0.78	0.79	1.01

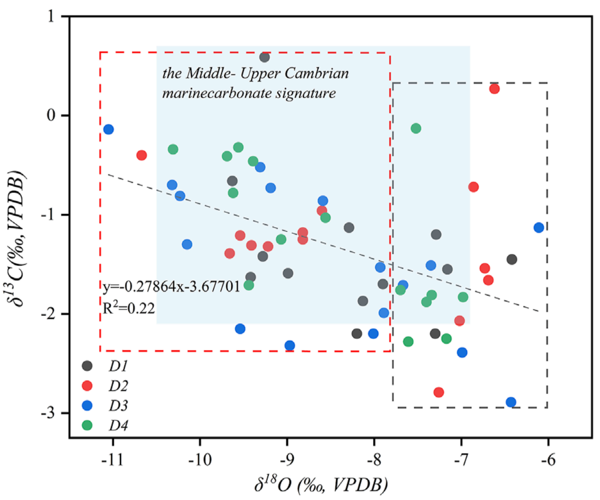

FIGURE 7
Cross-plot of $\delta^{13}C$ vs. $\delta^{18}O$ of different types of dolomites in the Xixiangchi Formation. The red dashed line represents the data of Southern Sichuan, and the black dashed line represents the data of Central Sichuan.

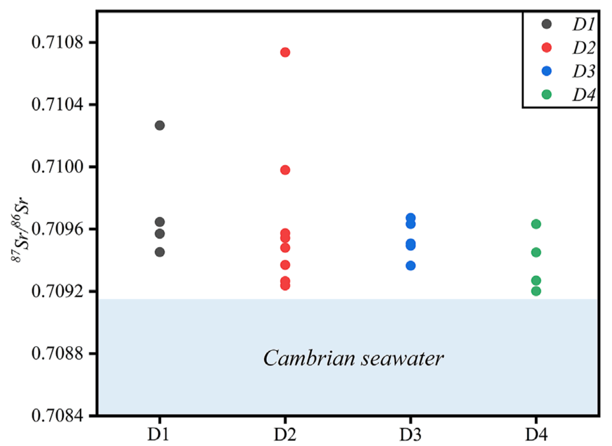

FIGURE 8
$^{87}Sr/^{86}Sr$ ratios of different types of dolomites in Xixiangchi Formation. The $^{87}Sr/^{86}Sr$ ratios of the Cambrian seawater are from (Denison, et al., 1998).

(82.1 ± 41.1 ppm, n = 3); and in D4, it is 34.7–151.3 ppm (75.5 ± 45.1 ppm, n = 4) (Table 1).

From the Fe-Mn cross plot of the Central - Southern Sichuan Basin area, it can be seen that the Fe-Mn content of D1-D4 dolomite shows a gradually increasing trend (Figure 9).

4.2.3.3 Rare earth elements

Standardized reference materials including Post-Archean Australian Shale (PAAS), North American Shale Composite (NASC), and CI chondrite have been widely adopted for REE data normalization (Wang, 2015; Jiang et al., 2023). This study employs PAAS normalization with “SN” notation for standardized values (Figure 10).

4.2.3.3.1 Central Sichuan basin D1 (n = 3) exhibits ΣREE = 11.2–21.5 ppm (14.96 ± 5.66) with $(Nd/Yb)_{SN}$ = 0.38–0.61 (0.53 ± 0.13), indicating HREE enrichment. PAAS-normalized patterns show weak negative Ce anomalies (Ce/Ce^*= 0.73–0.94, 0.86 ± 0.01) and near-unity Eu anomalies (Eu/Eu^*= 0.89–1.12, 0.99 ± 0.12). D2 (n = 4) demonstrates ΣREE = 6.8–23.2 ppm (11.56 ± 7.09) with $(Nd/Yb)_{SN}$ = 0.53–1.02 (0.80 ± 0.17), maintaining HREE-enriched characteristics. Ce/Ce^*= 0.89–1.02 (0.96 ± 0.06) and Eu/Eu^*= 0.67–1.20 (0.94 ± 0.13). D3 (n = 4) shows ΣREE = 7.94–21.05 ppm (13.56 ± 4.73) and $(Nd/Yb)_{SN}$ = 0.53–0.70 (0.61 ± 0.06), continuing

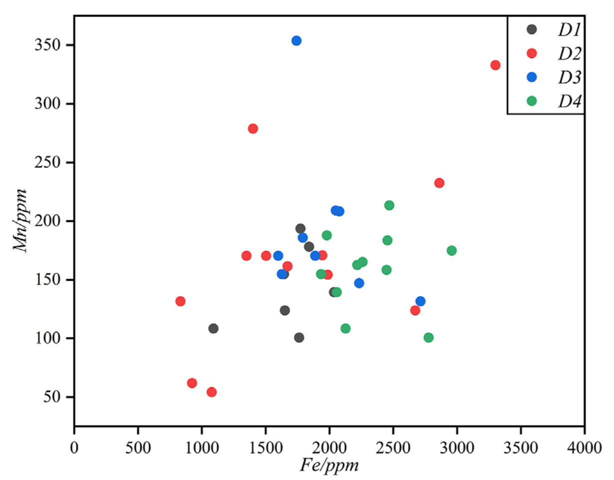

FIGURE 9
Cross-plot of Fe-Mn in the study area.

HREE enrichment trends. Notable positive Eu anomalies (Eu/Eu*= 0.92–1.01, 1.00 ± 0.03) occur with Ce/Ce*= 0.93–0.99 (0.96 ± 0.02). D4 (n = 2) has ΣREE = 10.31 ± 2.13 ppm and $(Nd/Yb)_{SN}$ = 0.81 ± 0.22, displaying flat PAAS-normalized patterns with weak Ce (0.94 ± 0.02) and Eu anomalies (0.95 ± 0.1). Hydrothermal influence is evidenced by sporadic positive Eu anomalies.

4.2.3.3.2 Southern Sichuan Basin Sample D1 (n = 16) exhibits ΣREE concentrations ranging from 4.75 to 23.01 ppm (average 8.2 ± 2.3) with $(Nd/Yb)_{SN}$ ratios of 0.44–1.19 (average 1.03 ± 0.29), indicating LREE enrichment compared to the central basin. It shows Ce/Ce*ratios of 0.91–0.98 (average 0.94 ± 0.03) and pronounced negative Eu anomalies (Eu/Eu*= 0.50–0.60, average 0.57 ± 0.04).

Sample D2 (n = 5) displays ΣREE concentrations ranging from 5.48 to 23.21 ppm (average 10.85 ± 6.5) and elevated $(Nd/Yb)_{SN}$ ratios of 1.06–1.52 (average 1.25 ± 0.06), further emphasizing LREE-enriched characteristics. It shows reduced Eu anomalies (Eu/Eu*= 0.62–0.89, average 0.75 ± 0.09) alongside Ce/Ce*ratios of 0.84–0.99 (average 0.92 ± 0.06).

Sample D3 (n = 3) exhibits lower ΣREE concentrations ranging from 5.23 to 10.53 ppm (average 7.8 ± 2.17) with sustained LREE enrichment ($(Nd/Yb)_{SN}$ = 1.14–1.28, average 1.21 ± 0.06). It shows Ce/Ce*ratios of 0.83–0.97 (average 0.89 ± 0.06) and weak Eu anomalies (Eu/Eu*= 0.77–0.80, average 0.79 ± 0.01).

Sample D4 (n = 5) shows ΣREE concentrations ranging from 6.88 to 12.19 ppm (average 9.6 ± 2.05) with $(Nd/Yb)_{SN}$ ratios of 1.07–1.42 (average 1.25 ± 0.13), maintaining LREE-enriched patterns. Minimal anomalies are observed with Ce/Ce*ratios of 0.78–0.96 (average 0.90 ± 0.07) and Eu/Eu*ratios of 0.79–0.99 (average 0.87 ± 0.08).

5 Discussion

5.1 Data validation

As a typical chemical sedimentary rock, carbonate rocks can effectively record the geochemical characteristics of rare earth elements (REEs) during their formation. Studies have shown that REE ions in the +3 valence state exhibit good chemical stability during their migration from the fluid phase to the crystal lattice of carbonate minerals (Nothdurft et al., 2004; Webb and Kamber, 2000; Özyurt et al., 2020).

However, it is worth noting that carbonate sedimentary systems are often not completely pure and frequently incorporate terrigenous clastic components such as silicate minerals and Fe-Mn oxides/hydroxides (Zhao et al., 2009). The incorporation of these exogenous substances may significantly affect the REE partitioning patterns of carbonate rocks (Özyurt, et al., 2023).

During the selection of experimental samples, we first employed thin-section analysis to identify specimens with uniform mineral grains, no evident dissolution pores, or cement infillings. Samples containing abundant secondary minerals (e.g., quartz, pyrite, clay minerals) or those exhibiting recrystallization features (e.g., coarse grains with straight grain boundaries) were avoided, as such minerals often indicate late-stage fluid alteration. Additionally, we prioritized the matrix (fine-grained primary sedimentary components) over cement (coarse crystalline minerals precipitated during late diagenesis), as the latter is more likely to have experienced geochemical modifications. By integrating these criteria with geochemical indicators to screen out samples with significant alteration, the selected specimens are deemed suitable for geochemical elemental analysis. Previous research has confirmed that when the silicate content reaches 1%, it can significantly alter the REE distribution characteristics of carbonate rocks, weakening or even eliminating their geochemical anomaly signals (Zhao and Zhen, 2017). Based on previous research results (Zhao et al., 2019), this study used trace elements Sc and Th as indicators to determine the degree of terrigenous material contamination, setting the screening criteria as Sc content <2 ppm and Th content <0.5 ppm. After systematically screening and removing contaminated samples, the reliability of the data was further verified through correlation analysis between REEs and the contents of TiO_2, MnO, Fe_2O_3, and SiO_2 (Figure 11). These data indicate that the REE model is mainly modified by diagenetic fluids rather than by clastic input. The results showed no significant correlation between REE contents and the above oxides in the strictly screened samples, confirming data reliability. The specific data can be found in Table 1.

Carbonate rocks may undergo diagenetic alteration during their formation, losing original sedimentary information. This study also evaluated diagenetic alteration of the samples. It is generally believed that when the Mn/Sr ratio is less than 3, carbonate rocks have not undergone obvious diagenetic alteration. When the Mn/Sr ratio is less than 10.0, although carbonate rocks have experienced a certain degree of diagenetic transformation, they usually still retain original marine information. In this study, the Mn/Sr ratios of matrix dolomites range from 0.60 to 4.19, with an average of 2.53. Therefore, based on the characteristics of Mn/Sr ratios in the dolostone samples of the Xixiangchi Formation, it can be seen that the selected samples in this study experienced diagenetic alteration, and these dolostones still retain their primary carbon and oxygen isotope signatures. Fölling and Frimmel (2002) proposed that carbonate samples with $\delta^{18}O > -10‰$ show no obvious diagenetic alteration, and this criterion was used for evaluation. Most samples in this study have $\delta^{18}O$ values > −10‰ (only a few are slightly lower), and considering that the $\delta^{18}O$ values of Middle-Late Cambrian seawater

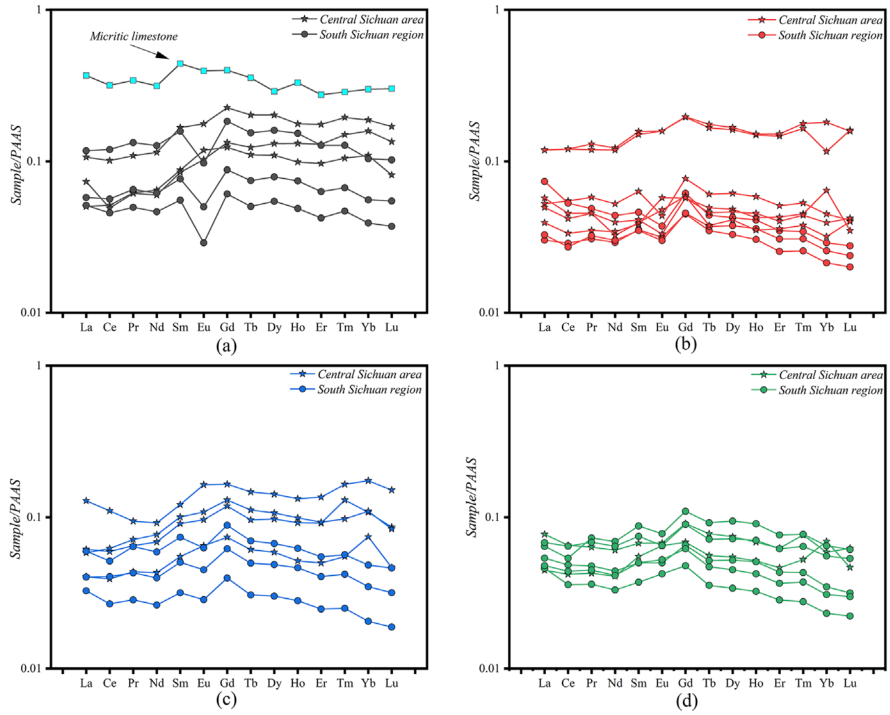

FIGURE 10
PAAS-normalized REEs partition patterns of different types of the examined D1 **(a)**, D2 **(b)**, D3 **(c)**, D4 **(d)**, dolomites in the Xixiangchi Formation and micritic limestone.

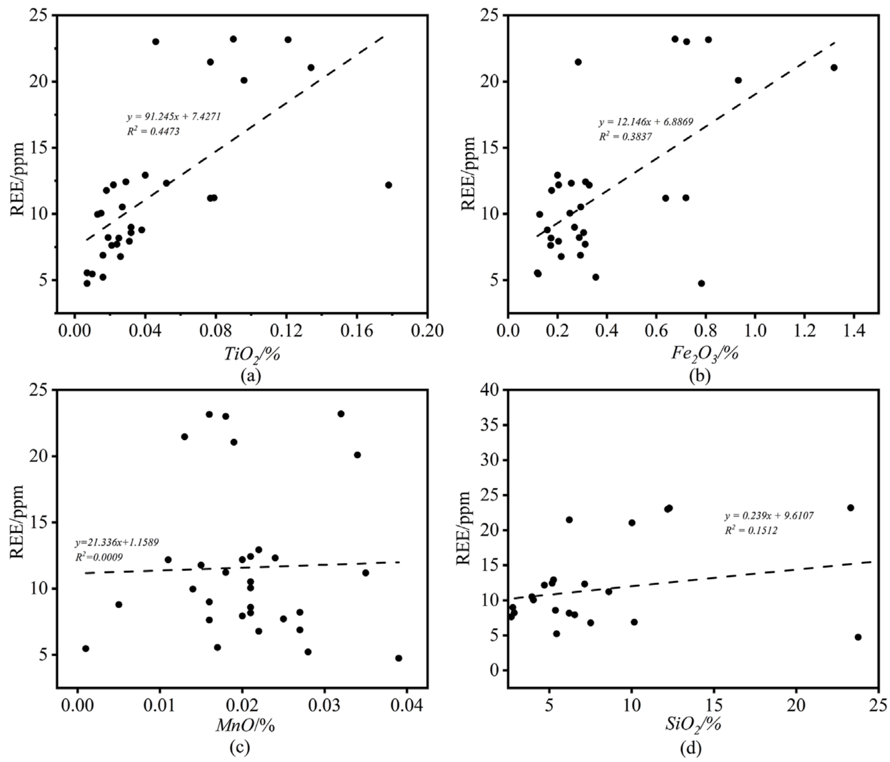

FIGURE 11
Cross-plot of **(a)** TiO_2 concentration, **(b)** Fe_2O_3 concentration, **(c)** Mn concentration, and **(d)** SiO_2 concentration with with ΣREE of the investigated Xixiangchi dolomites.

range from −10.5‰ to −6.9‰ (Veizer et al., 1999), carbonate rocks may still preserve their original isotopic signals even when $\delta^{18}O$ is marginally below −10‰ (Zhang et al., 2022). Additionally, the correlation between $\delta^{13}C$ and $\delta^{18}O$ values of carbonate rocks can indicate diagenetic alteration: when marine carbonates show no significant positive correlation between $\delta^{13}C$ and $\delta^{18}O$, their original carbon and oxygen isotopic characteristics are considered preserved (Kaufman et al., 1991; Veizer et al., 1999). In this study, the $\delta^{13}C$ and $\delta^{18}O$ values of samples show no significant covariance (Figure 8), indicating that the samples as a whole have retained the primary isotopic information.

5.2 Diagenetic fluid analysis

The $\delta^{13}C$ values for D1–D4 (−1.39‰ ± 0.67‰ to −1.22‰ ± 0.3‰) fall within the Middle–Upper Cambrian marine carbonate range (−2.1‰–0.7‰; Veizer et al., 1999), supporting seawater-derived dolomitizing fluids. The$\delta^{18}O$ values (−8.41‰ ± 1.07‰ to −8.63‰ ± 1.19‰) also align with contemporaneous marine carbonates (−6.9‰–10.5‰; Veizer et al., 1999) and published data from the Xixiangchi Formation (Jia et al., 2017; Li W. Z. et al., 2019; Ren et al., 2022). Among them, the burial depth of dolomites increases from D2 and D3 to D4. Compared with the marine carbonates of the Middle-Upper Cambrian, their $\delta^{18}O$ values show negative deviation characteristics, possibly caused by the increase in burial temperature. The reason for the negative deviation in $\delta^{18}O$ values of D1 may be due to its location in the near-surface environment, subject to the slight influence of atmospheric fresh water. Theoretically, the dolomitization of fresh water-seawater mixing can also cause the negative deviation of $\delta^{18}O$ values in mixed water dolostones. During the Xixiangchi Formation period, the climate was relatively hot and the evaporation was strong. In such environmental conditions, the atmospheric fresh water required for large-scale dolomitization was lacking, making it impossible for large-scale fresh water-seawater mixing dolomitization to occur. Allan and Wiggins (1993) and Meyera et al. (1997) have conducted special studies on the C and O isotope geochemistry of mixed water dolostones and concluded that the $\delta^{18}O$ and $\delta^{13}C$ values vary greatly, and this variation shows a "positive linear correlation", that is, the $\delta^{18}O$ value increases with the increase of $\delta^{13}C$ value, or decreases with the decrease of $\delta^{13}C$ value. However, it can be seen from Figure 7 that the $\delta^{13}C$ and $\delta^{18}O$ values lack such a positive linear distribution relationship.The $^{87}Sr/^{86}Sr$ ratios of Xixiangchi Formation dolomites (D1: 0.70973 ± 0.00031; D2: 0.70965 ± 0.00042; D3: 0.70953 ± 0.00011; D4: 0.70939 ± 0.00015) exceed contemporaneous Cambrian seawater values (0.70840–0.70915; Denison et al., 1998). The downward trend from D1 to D4 reflects diminishing silicate and clay mineral influences, with D4 values approaching seawater ranges (Figure 8). Specifically, D1's elevated $^{87}Sr/^{86}Sr$ suggests strong silicate/clay interactions, while D3–D4 trends correlate with burial-driven closure of the diagenetic system. D2's lower ratio may relate to high-energy environments inhibiting silicate mixing.

Fe and Mn preferentially substitute for Ca^{2+} and Mg^{2+} under reducing conditions due to their similar ionic radii. From D1 to D3/D4, Fe and Mn concentrations progressively increase (Figure 9), indicating enhanced fluid reductivity and a transition toward more closed diagenetic environments.

Due to its multivalence, Ce is sensitive to redox conditions and is widely used to reflect the redox state of seawater (Azmy et al., 2011). Ce^{3+} is soluble, but when the water body is oxidized, Ce^{3+} is easily oxidized to insoluble Ce^{4+}, which is less mobile and tends to adsorb onto Fe-Mn oxides, organic matter, or clay particles (Bau and Dulski, 1996). This leads to its separation from other trivalent rare earth elements, causing a negative Ce anomaly in the sedimentary water. In the dolomites of the Xixiangchi Formation, the Ce anomaly values for D1, D2, D3, and D4 are 0.91 ± 0.07, 0.92 ± 0.06, 0.93 ± 0.05, and 0.91 ± 0.06, respectively (Table 1), all exhibiting weak negative anomalies consistent with the characteristics of Ce anomalies in seawater. The Ce anomalies in the matrix dolomites D1, D2, D3, and D4 are very close, indicating that their dolomitizing fluids likely had similar sources and formed in a weakly oxidizing environment, such as near-surface to shallow burial environments.

Similar to Ce, Eu also exhibits multivalent characteristics and is sensitive to redox conditions. Under reducing conditions, Eu^{3+} in fluids is typically reduced to Eu^{2+}, thus separating it from other trivalent rare earth elements. However, because the ionic radius of Eu^{2+} is closer to that of Ca^{2+}, Eu more easily substitutes for Ca^{2+} to enter the carbonate lattice. The redox potential of Eu^{2+}/Eu^{3+} is primarily controlled by temperature (Bau, 1991), decreasing with increasing burial temperature. Generally, the presence of positive Eu anomalies in carbonates requires two conditions: reducing fluids and diagenetic fluid temperatures exceeding 200°C (Bau and Dulski, 1996; Debruyne et al., 2016). Therefore, positive Eu anomalies in dolostones are often used to indicate high-temperature hydrothermal dolomitization events (Parsapoor et al., 2009; Bau et al., 2010). When high-temperature hydrothermal fluids mix with large amounts of seawater, the temperature may decrease, but positive Eu anomalies may be preserved (Bau et al., 2010). Notably, Eu anomalies can also characterize water-rock alteration at relatively low temperatures, especially in environments of seawater-basalt interaction (Özyurt and Kırmacı, 2025). In the dolostones of the Xixiangchi Formation, negative Eu anomalies occur in D1, D2, D3 and D4, with average values of 0.73 ± 0.21, 0.83 ± 0.17, 0.91 ± 0.12 and 0.92 ± 0.09, respectively (Table 1), indicating that dolomitization was not affected by hydrothermal fluids. Moreover, from D1 to D2, D3, and D4, Eu anomaly gradually intensifies, reflecting the gradual increase in diagenetic fluid temperature during burial.

The abundances and distribution patterns of rare earth elements (REEs) can indicate the diagenetic fluids, material sources, and formation environments of carbonates (Jiang et al., 2016a). The REE distribution pattern in modern marine water phases exhibits a distinct left-leaning pattern, characterized by LREE depletion, HREE enrichment, and negative Ce anomaly (Nothdurft et al., 2004). Normal marine carbonates generally inherit the REE distribution pattern of seawater to some extent and typically show similar characteristics. The REE distribution patterns of D1, D2, D3, and D4 are highly similar, all displaying nearly flat patterns with slight LREE enrichment, slight HREE depletion, weak negative Ce anomalies, and negative Eu anomalies. The difference between the flat partitioning pattern in the study area and the REE partitioning pattern in seawater may be related to the different ionic radii of REE. During the diagenetic stage, rare earth elements may be released from mudstone, organic matter, clastic particles, and unstable minerals into pore fluids, leading to an increase in REE content and possibly forming a flat partitioning pattern (Jiang et al., 2016b). Furthermore, when interpreting rare earth element partitioning patterns, it is often necessary to introduce the seawater partitioning pattern for comparative analysis to determine whether the diagenetic fluid is related to seawater. The micritic limestone in the study area has a dense lithology, has not undergone obvious diagenetic modification, and well preserves the original seawater information. Therefore, its rare earth element partitioning pattern can be used to represent the partitioning pattern of seawater in the same period (Qing and Mountjoy, 1994). Through analysis of the REE distribution patterns of various rock types in the study area, the dolomites in the southern Sichuan Basin strata all exhibit slightly right-inclined characteristics of light rare earth elements (LREE) enrichment and heavy rare earth elements (HREE) depletion, similar to the distribution patterns of micritic limestones (Figure 9). This indicates that the dolomites in the study area share the same fluid source as micritic limestones. As micritic limestones represent the characteristics of original seawater, it can be inferred that dolomitization originated from contemporaneous marine-derived fluids. Additionally, this suggests that the dolomites were less affected by other non-marine fluids during their formation, reflecting a relatively closed diagenetic system. In central Sichuan Basin, however, left-inclined characteristics of weak LREE depletion and weak HREE enrichment are displayed, well preserving the distribution characteristics of modern seawater. This also indicates that the central Sichuan area was located in a high-energy zone, relatively less affected by argillaceous or organic clastic particles and unstable minerals.

5.3 Reservoir genesis and main controlling factors

5.3.1 Tectono-sedimentary characteristicsand the control over reservoir development

During the deposition of the Xixiangchi Formation in the Sichuan Basin, there was a stable cratonic sedimentary belt that retained the paleogeographic patterns of the Early-Middle Cambrian period. This included platform flats with peripheral basins along the northern and eastern margins (Jing et al., 2016; Gu et al., 2020). The limited input of terrestrial material from western paleocontinents (Kangdian, Motianling, Hannan) resulted in mixed tidal flat deposits being restricted to proximal paleoland areas, while clear-water, shallow-water carbonate dominated the platform interiors. The depositional environments primarily consisted of restricted and open platform facies, which included lagoon subfacies and intra-platform shoal subfacies.

Residual thickness analysis reveals northwest-thinning, and southeast-thickening trends of the Xixiangchi Group in the central Sichuan Basin. The Leshan-Longnvsi paleo-uplift tectonic belt (with its core at the Moxi area, southeastern limb) controls the depositional architecture (Wang et al., 2008). Arelative sea-level decline positioned paleo-uplift core areas near high-energy wave base surfaces, initiating intra-platform shoal development. At the same time, elevated paleo-uplift limb regions emerged above wave base, enabling shoal formation. As sea level progressively fell, denudation fronts shifted towards limbs, terminating shoal growth at early high-standing areas while sustaining development in accommodation-rich limb depressions. This process generated ring-shaped shoal belts around paleo-uplifts, with greater cumulative thicknesses in paleohighs and underwater high limbs compared to core shallow-water zones.

Southern Sichuan Basin exhibits deeper paleowater depths than central regions, dominated by grain dolomite and crystalline dolomite lithologies with subordinate conglomeratic dolomite interbeds. Shoals primarily occur as platform-margin or intra-platform types along lagoon peripheries and southeastern slope-break zones. Original porosity development, strongly facies-controlled, proves critical for reservoir quality. High-energy platform-margin and intra-platform shoals generate grain-supported carbonate frameworks that constitute essential reservoir precursors in the Southern Sichuan Basin.

The interplay between structural-sedimentary controls and reservoir development is evident, with carbonate grain shoals serving as the foundation for high-quality reservoirs. Integrated analysis of sedimentary-tectonic characteristics in the Xixiangchi Formation demonstrates that paleo-uplifts and syndepositional faults dominantly control grain shoal distribution.

Multi-phase tectonic events from the Caledonian to Himalayan orogenies have shaped the Sichuan Basin's Cambrian strata, creating stratigraphic unconformities and prominent paleo-uplifts including the Central Sichuan, Northern Sichuan, and Qianzhong Paleo-Uplifts. These paleo-uplifts exhibit abrupt topographic margins that facilitate high-energy hydrodynamic conditions, particularly evident in the preferential distribution of Longwangmiao Formation reservoirs along uplift slopes and platforms. Syndepositional uplift during the Tongwan Movement (late Sinian-Early Cambrian) established a southwest-high, northeast-low paleogeomorphic framework, further enhanced by subsequent Xingkai Movement-induced differential subsidence.

Depositional facies fundamentally govern reservoir heterogeneity through dual mechanisms. High-energy environments (platform margins/intra-platform shoals) develop well-sorted grainstones with 15%–25% primary porosity through active hydrodynamic flushing, whereas low-energy micritic deposits exhibit minimal pore development. Lithological composition determines diagenetic potential: grain-dominated dolomites retain dissolution-enhanced porosity, while microcrystalline dolomites remain tight (<3% porosity) with limited intercrystalline pores. This facies-controlled porosity hierarchy underscores the material basis provided by platform-edge shoals for reservoir development. Syndepositional faults like the Qiyueshan Fault enhanced late-stage geomorphic differentiation, creating slope-break zones conducive to platform-margin shoal formation through underwater sediment partitioning (Figure 12).

5.3.2 Control of diagenesis on reservoir development

5.3.2.1 Compaction-pressure solution

Compaction and pressure solution predominantly occur in burial diagenetic environments, as evidenced by the presence of stylolites exhibiting bedding-parallel distribution in vertical profiles. While stylolites reduce primary porosity by providing material sources for calcite cementation, they may later act as hydrocarbon migration pathways and reservoir spaces through subsequent

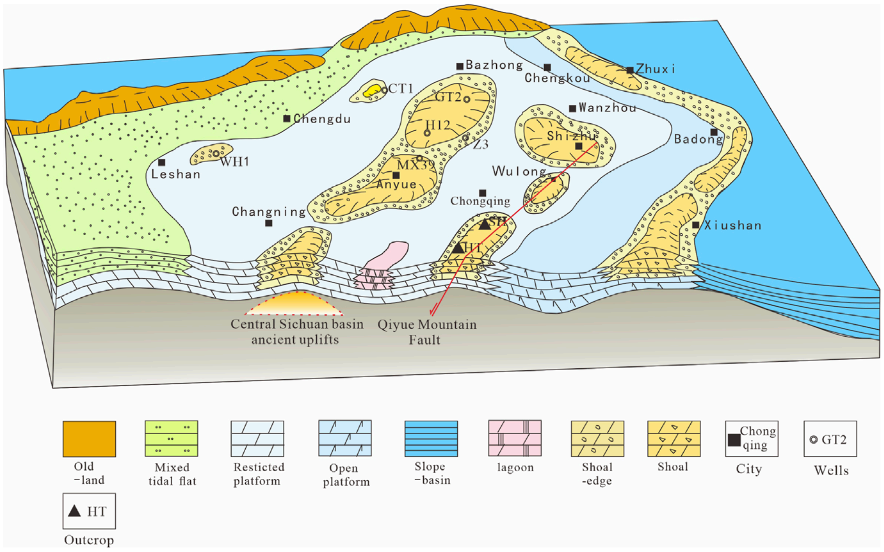

FIGURE 12
The structural-depositional evolution model diagram of Xixiangchi Formation (were modified after Wen et al., 2022).

dissolution or tectonic modification, demonstrating a dual role in reservoir quality evolution.

5.3.2.2 Cementation

Dolomite cements in D3 and D4 exhibit fog-core and bright-rim textures, indicative of burial fluid-mediated recrystallization. These cements partially fill intergranular and dissolved pores, reducing primary porosity. If residual pores remain between the crystal grains following dolomite cementation, these pores represent one of the primary pore types within the Xixiangchi Formation reservoir in the study area.

5.3.2.3 Dolomitization

The texture of D1 is relatively dense, mostly with laminated structures, and gypsum veinlets are developed (Figure 3i). Laminated structures typically form in low-energy tidal flat environments. The low contents of Mn and Sr suggest it may have formed in a weak oxidizing near-surface environment, possibly influenced by atmospheric fresh water leading to low Sr content. Compared with other types of dolomites, D1 has lower $\delta^{13}C$ values and the highest $\delta^{18}O$ values, with carbon-oxygen isotopic values mostly within the range of marine carbon-oxygen isotopes, indicating that D1 overall formed in a marine environment with near-surface fresh water influence. The average ΣREE of D1 is relatively high, and its distribution pattern shows characteristics of weak LREE enrichment, weak HREE depletion, negative Ce anomaly, and negative Eu anomaly, suggesting that D1 formed in an oxidizing and low-temperature diagenetic environment. Therefore, it is inferred that D1 is a dolomitization product under the penecontemporaneous evaporation-concentration model (Jiang, et al., 2015; Jiang et al., 2016a). It is mainly located in a near-surface environment with strong evaporation and relatively high salinity. Due to continuous evaporation, the deposited seawater continuously moves upward and concentrates under evaporation, increasing the Mg^{2+}/Ca^{2+} ratio in seawater, which replaces carbonate minerals to form D1 (Zhou, et al., 2024).

D2 has a residual granular texture, with fine-powder crystalline subhedral dolomite cement between sand-sized clasts, mainly sparry cement, indicating its depositional environment was a high-energy beach facies. The $\delta^{13}C$ and $\delta^{18}O$ of residual granular dolomite are also consistent with the characteristics of Middle-Late Cambrian marine carbonates. The ΣREE value of D2 is lower than that of D1, with a similar nearly flat REE distribution pattern, indicating stronger dolomitization and a fluid source similar to D1. However, the Ce anomaly is slightly weakened trend may reflect a gradual decrease in the oxidizing nature of the diagenetic environment and a gradual increase in temperature. Therefore, it is speculated that D2 may have formed through permeation-reflux dolomitization. It is overall located in a high-energy beach zone with good permeability, eroded by seawater and atmospheric fresh water, forming numerous intergranular pores. Subsequently, in the shallow burial environment, Mg^{2+}-rich brine from the upper part infiltrated downward to cause permeation-reflux dolomitization, forming D2.

Microfractures filled with asphalt are visible inside D3, indicating it may have been in a burial environment. Compared with D2, the Fe and Mn contents in D3 (1968.74 ± 331.0 ppm and 192.4 ± 62.1 ppm, respectively) are higher, reflecting enhanced reducibility of the dolomitizing fluid. The $\delta^{13}C$ and $\delta^{18}O$ values are close to those of D2. In addition, the ΣREE value of D3 is lower than those of D1 and D2, possibly due to more complete dolomitization. It has a relatively flat distribution pattern, similar to D1 and D2, indicating that its dolomitizing fluid originated from seawater or marine-derived fluids. The Ce anomaly is weaker than those in D1 and D2, while the Eu anomaly is stronger than the former two, reflecting the gradual increase in the reductivity of the diagenetic environment and temperature, that is, the burial depth gradually increases Therefore, it is speculated that the powder crystalline dolomite of the Xixiangchi Formation in the study area formed by burial dolomitization during the burial period, with its diagenetic fluids mainly being downward-migrating marine-derived fluids and seawater remaining in pores.

D4 has residual granular phantom and fog-core bright-edge textures, speculated to be recrystallized from D2, and stylolites are visible inside. This is consistent with the characteristic of high dolomitization degree indicated by its lowest ΣREE value. The $\delta^{13}C$ value in D4 indicates marine-derived fluid characteristics, while the further negative shift in $\delta^{18}O$ value also confirms an increase in dolomitization environment temperature. Similarly, its distribution pattern is similar to that of the other three types of dolomites and micritic limestones, indicating similarity in diagenetic fluids, presumably derived from seawater remaining between layers. The relatively negative deviation in bulk $\delta^{18}O$ values of D4 suggests it may have been influenced by hydrothermal fluids in fractures, forming saddle dolomite cements, however, Eu exhibits a negative anomaly. Possible reasons may be that the hydrothermal temperature was lower than 200°C, thus causing the negative deviation in $\delta^{18}O$ values while Eu remains negatively anomalous. Meanwhile, the average $^{87}Sr/^{86}Sr$ value (0.70939 ± 0.00017) is close to those of the previous dolomite types, showing certain inheritance. Therefore, D4 is considered to have formed through overgrowth or recrystallization of pre-existing dolomite under higher temperature and pressure conditions in the shallow-to-moderate burial environment, with its Mg^{2+} possibly derived from basin fluids stored in intercrystalline pores and may have been influenced by hydrothermal fluids migrated up through fractures.

5.3.2.4 Dissolution

Dissolution significantly enhances reservoir quality through three developmental phases (Xiong and He, 2022). The initial penecontemporaneous phase occurs in vadose-zone conditions during early diagenesis, where selective dissolution of metastable components generates intragranular and moldic pores (Figure 3b). These primary pores become occluded by subsequent granular cementation. The predominant supergene phase, associated with Caledonian tectonic uplift-induced denudation, drives intense karstification in the Xixiangchi Formation. This process creates intergranular/intercrystalline dissolution pores, bedding-parallel dissolution cavities, and fracture networks, with paleokarst breccias (Figure 3h) comprising the principal effective porosity system. The final burial phase involves acidic fluids (organic acids, CO_2) modifying pre-existing structural fractures and stylolites, forming secondary dissolution features containing residual bitumen (Wang, 2019; Figure 3e), particularly enhancing fracture connectivity rather than generating new pore volume.

5.3.2.5 Fracturing

Fractures serve dual roles in carbonate reservoirs as both storage spaces and critical conduits for hydrocarbon migration. The study area has undergone multiphase tectonic deformation, including the Caledonian, Yunnan, Dongwu, Indosinian, Yanshan, and Himalayan movements, resulting in high-angle structural fractures and horizontally developed fracture networks (Figure 3i). Synergistic interaction between fracturing and large-scale karstification generates effective fracture systems, with subsequent dissolution enhancing their connectivity through dissolution-enhanced fractures (Figure 3j). These fracture networks not only directly improve reservoir permeability but also interconnect pre-existing pores, facilitating fluid migration that promotes secondary porosity development—a key mechanism for improved reservoir quality in the study area.

5.4 Dolomitization mechanism and reservoir porosity formation

During the Middle-Late Cambrian Xixiangchi Period, the study area largely retained the west-high-east-low paleogeographic framework of the Longwangmiao and Gaotai Periods. The Xixiangchi Period saw a complete transgressive-regressive sedimentary cycle, featuring rapid early transgression followed by slow regression (Li et al., 2008), within a predominantly restricted platform environment. Paleotectonic studies indicate the Sichuan Basin was positioned at 30°N, 105°E during the Cambrian, under warm subtropical climates with strong evaporation. Sea-level fall and evaporation enabled penecontemporaneous dolomitization via pump suction in supratidal zones, forming D1 dolostones. Concurrently, in restricted settings, gravitationally driven downward migration of evaporative seawater through high-permeability shoals induced seepage-reflux dolomitization, generating D2 dolostones. Successive sea-level declines shifted dolomitization seaward, repeatedly forming D1-D2 couplets—explaining the dominance of D1/D2 replacement in most Xixiangchi Formation sediments. In near-surface to shallow burial environments, Mg^{2+}sourced from residual pore water and downward-percolating seawater, combined with increasing temperature-pressure, overcame kinetic barriers to drive dolomitization and recrystallization, forming D3 dolostones. Following a brief Caledonian uplift, deeper burial increased thermobaric conditions, promoting overgrowth/recrystallization of early dolomites and reducing porosity. Depletion of Mg^{2+} during early dolomitization limited mid-burial stage sources, restricting D4 overgrowth/recrystallization to localized zones, hence its rare occurrence in the study area.

The carbonate rocks of the Xixiangchi Formation underwent early diagenetic processes including cementation, penecontemporaneous dolomitization, and atmospheric freshwater dissolution under shallow marine and surface seepage environments. Initial dissolution porosity was partially reduced by rapid pore-filling processes. Previous studies indicate that carbonate rocks typically exhibit primary porosity of 40%–70% (Choquette and Pray, 1970), with syngenetic to penecontemporaneous cementation and filling significantly reducing pore space. Although moldic and dissolution pores enhanced reservoir quality to some extent, petrographic analysis of particle contact relationships in microphotographs suggests that reservoir porosity reduced to less than 15% during this stage. As burial depth and temperature increased, the Xixiangchi Formation transitioned into a semi-closed to closed shallow-medium burial environment. Early-formed dolomites underwent recrystallization, producing both coarse-grained euhedral crystals and fine-grained subhedral to anhedral crystals through differential recrystallization processes. This stage was characterized by compaction, recrystallization, cementation, and tectonic fracturing, further reducing dolomite reservoir porosity to 8%–10%. During the late Caledonian

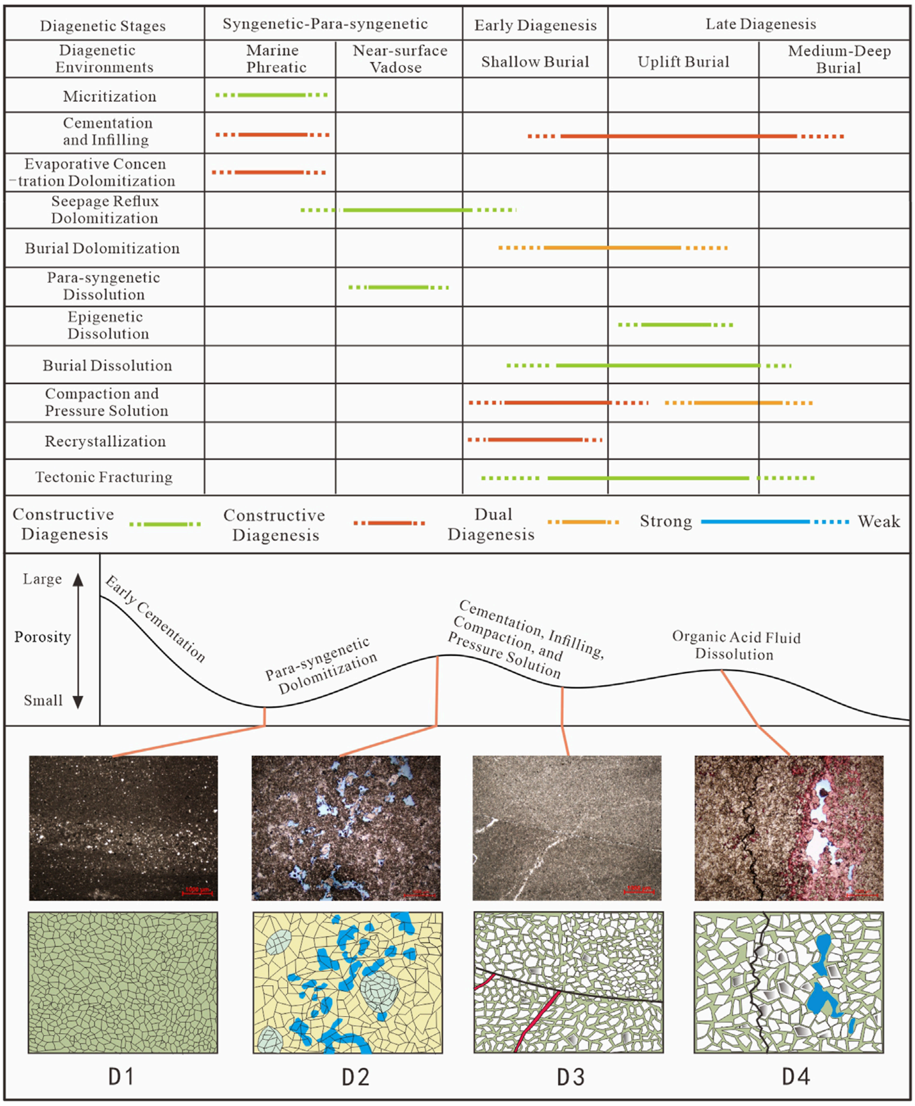

FIGURE 13
Diagenetic sequence and pore evolution of dolomite reservoirs of Cambrian Xixiangchi Formation in Sichuan Basin (were modified after Li et al., 2022).

period, regional uplift of the Leshan-Longnvsi paleo-uplift created an open diagenetic environment. Epigenetic karstification through atmospheric freshwater and groundwater interaction generated extensive dissolution pores and vugs in the upper Xixiangchi Formation. Concurrent tectonic uplift enhanced reservoir permeability through structural fracture development while facilitating fluid migration. Reservoir porosity increased to an estimated 10%–12% during this stage, based on subsequent filling intensity. During the middle-deep burial stage, the Xixiangchi Formation dolomites were completely isolated from oxidizing conditions. The progressive increase in burial depth and temperature/pressure conditions led to pressure dissolution and a reduction in porosity. While acidic fluids (CO_2 and organic acids) improved reservoir quality by dissolving minerals at intermediate depths, the subsequent precipitation of hydrothermal minerals (such as calcite, saddle dolomite, and quartz) from deep ascending fluids filled most of the secondary porosity. This final diagenetic phase resulted in observed reservoir porosities of 3%–5% due to a combination of dissolution and precipitation processes (Figure 13).

6 Conclusion

(1) The Xixiangchi Formation reservoirs in the study area predominantly consist of microcrystalline dolomites, fabric-retentive dolomites, very finely to finely crystalline dolomites, and finely to medium crystalline dolomites as the main lithologies. The reservoir spaces exhibit dual porosity systems consisting of pore-type and fracture-type storage, dominated by intergranular dissolution pores, intragranular dissolution pores, intercrystalline pores, intercrystalline dissolution pores, and moldic pores. Core analysis reveals an overall low-porosity, low-permeability reservoir system, although localized high-porosity, high-permeability zones alongside low-porosity,

high-permeability intervals occur in central Sichuan Basin sectors. Reservoir types are predominantly fracture-pore systems, with isolated pore-dominated reservoirs developing in specific structural domains.

(2) The diagenetic evolution of the Xixiangchi Formation reflects complex polyphase tectonic influences. Integrated microphotographs petrography and core analysis identify four principal diagenetic processes: cementation, dolomitization, dissolution, and fracturing. Combined lithological observations with geochemical data constrain three distinct dolomitization mechanisms: 1) Evaporative-concentration dolomitization during syngenetic-penecontemporaneous stages formed microcrystalline dolomites, and 2) Seepage-reflux dolomitization under near-surface–shallow burial conditions generated fabric retentive dolomite. 3)Subsequent medium-deep burial processes transformed precursor dolomites through recrystallization, producing very finely to finely crystalline dolomite and finely-medium crystalline dolomite via burial dolomitization or crystal coarsening.

(3) Reservoir development analysis identifies grain shoals as fundamental depositional controls, with two principal shoal-constrained mechanisms: paleo-uplift-controlled shoals and fault-controlled shoals. Sedimentary architecture and diagenetic modification emerge as dual controls on reservoir quality, where dolomitization preserves primary porosity through mineral stabilization. Dissolution serves as the primary enhancement mechanism for secondary porosity development, while fracture networks act as essential contributors to reservoir permeability enhancement. The interplay of these factors creates vertically heterogeneous but laterally continuous reservoir units.

Data availability statement

The original contributions presented in the study are included in the article/supplementary material, further inquiries can be directed to the corresponding author.

Author contributions

SC: Conceptualization, Writing – original draft. HW: Supervision, Writing – review and editing. XL: Data curation, Visualization, Writing – original draft. FH: Investigation, Writing – review and editing. BM: Investigation, Writing – review and editing. JL: Investigation, Resources, Visualization, Writing – review and editing. LD: Investigation, Resources, Visualization, Writing – review and editing.

Funding

The author(s) declare that financial support was received for the research and/or publication of this article. This study was supported by the SINOPEC Petroleum Exploration and Production Research Institute (NO.33550007-22-zc0613-0039) and Sichuan Science and Technology Program (NO.2025YFHZ0021). The authors declare that this study received funding from SINOPEC. The funder was not involved in the study design, collection, analysis, interpretation of data, the writing of this article, or the decision to submit it for publication.

Conflict of interest

The authors declare that the research was conducted in the absence of any commercial or financial relationships that could be construed as a potential conflict of interest.

Generative AI statement

The author(s) declare that no Generative AI was used in the creation of this manuscript.

Publisher's note

References

Al, N. Q. A., Sharbazheri, K. M. I., i Karim, K. H., and Ghafor, I. M. (2020). Cretaceous/paleogene boundary analysis by planktic foraminiferal biozonation in the western zagros fold- thrust belt (smaquli valley), sulaimani governorate, NE-Iraq. *Kirkuk Univ. J./Scientific Stud. (KUJSS)* 15 (3), 45–81. doi:10.32894/KUJSS.2020.15.3.3

Allan, J. R., and Wiggins, W. D. (1993). "Dolomite reservoirs: geo-chemical techniques for evaluating origin and distribution," in *AAPG continuing education course notes series No.36*. Tulsa: AAPG, 36–129.

Azmy, K., Brand, U., Sylvester, P., Gleeson, S. A., Logan, A., and Bitner, M. A. (2011). Biogenic and abiogenic low-Mg calcite (bLMC and aLMC): evaluation of seawater-REE composition, water masses and carbonate diagenesis. *Chem. Geol.* 280 (1-2), 180–190. doi:10.1016/j.chemgeo.2010.11.007

Badiozamani, K. (1973). The dorag dolomitization model, application to the middle Ordovician of Wisconsin. *J. Sediment. Res.* 43 (4), 965–984. doi:10.1306/74D728C9-2B21-11D7-8648000102C1865D

Barnaby, R. J., and Read, J. F. (1992). Dolomitization of a carbonate platform during late burial; lower to middle cambrian shady dolomite, Virginia appalachians. *J. Sediment. Res.* 62 (6), 1023–1043. doi:10.1306/D4267A3C-2B26-11D7-8648000102C1865D

Bau, M. (1991). Rare-earth element mobility during hydrothermal and metamorphic fluid-rock interaction and the significance of the oxidation state of europium. *Chem. Geol.* 93 (3-4), 219–230. doi:10.1016/0009-2541(91)90115-8

Bau, M., Balan, S., Schmidt, K., and Koschinsky, A. (2010). Rare earth elements in mussel shells of the Mytilidae family as tracers for hidden and fossil high-temperature hydrothermal systems. *Earth Planet. Sci. Lett.* 299 (3-4), 310–316. doi:10.1016/j.epsl.2010.09.011

Bau, M., and Dulski, P. (1996). Distribution of yttrium and rare-earth elements in the penge and kuruman iron-formations, transvaal supergroup, South Africa. *Precambrian Res.* 79 (1-2), 37–55. doi:10.1016/0301-9268(95) 00087-9

Choquette, P. W., and Pray, L. C. (1970). Geologic nomenclature and classification of porosity in sedimentary carbonates. *AAPG Bull.* 54 (2), 207–250. doi:10.1306/5d25c98b-16c1-11d7-8645000102c1865d

Davies, G. R., and Smith Jr, L. B. (2006). Structurally controlled hydrothermal dolomite reservoir facies: an overview. *AAPG Bull.* 90 (11), 1641–1690. doi:10.1306/05220605164

Debruyne, D., Hulsbosch, N., and Muchez, P. (2016). Unraveling rare earth element signatures in hydrothermal carbonate minerals using a source–sink system. *Ore Geol. Rev.* 72, 232–252. doi:10.1016/j.oregeorev.2015.07.022

Deng, C. K., Li, T., Yang, W. Q., Zhang, X. H., Cheng, Z. Z., Chen, H. R., et al. (2022). Characteristics and main controlling factors of shoal reservoirs in the middle-upper cambrian Xixiangchi Formation, central Sichuan Basin. *J. Of Palaeogeogr. Ed.* 24 (02), 292–307. doi:10.7605/gdlxb.2022.02.021

Denison, R. E., Koepnick, R. B., Burke, W. H., and Hetherington, E. A. (1998). Construction of the cambrian and ordovician seawater $^{87}Sr/^{86}Sr$ curve. *Chem. Geol.* 152 (3-4), 325–340. doi:10.1016/s0009-2541(98)00119-3

Dickson, J. A. D. (1966). Carbonate identification and genesis as revealed by staining. *J. Sediment. Res.* 36 (2), 491–505. doi:10.1306/74D714F6-2B21-11D7-8648000102C1865D

Elderfield, H. (1988). The oceanic chemistry of the rare-earth elements. *Philosophical Trans. R. Soc. Lond. Ser. A, Math. Phys. Sci.* 325 (1583), 105–126. doi:10.1098/rsta.1988.0046

Fölling, P. G., and Frimmel, H. E. (2002). Chemostratigraphic correlation of carbonate successions in the gariep and saldania belts, Namibia and South Africa. *Basin Res.* 14 (1), 69–88. doi:10.1046/j.1365-2117.2002.00167.x

Friedman, G. M., and Sun, S. Q. (1994). A reappraisal of dolomite abundance and occurrence in the Phanerozoic; discussion and reply. *J. Sediment. Res.* A64 (7), 360–362. doi:10.1306/d4268086-2b26-11d7-8648000102c1865d

Gomez-Rivas, E., Corbella, M., Martín-Martín, J. D., Stafford, S. L., Teixell, A., Bons, P. D., et al. (2014). Reactivity of dolomitizing fluids and Mg source evaluation of fault-controlled dolomitization at the Benicàssim outcrop analogue (Maestrat Basin, E Spain). *Mar. Petroleum Geol.* 55, 26–42. doi:10.1016/j.marpetgeo. 2013.12.015

Gu, M. F., Li, W. Z., Zou, Q., Zhou, G., Zhang, J. Y., Lü, X. J., et al. (2020). Lithofacies palaeogeography and reservoir characteristics of the cambrian Xixiangchi Formation in Sichuan Basin. *Mar. Origin Pet. Geol.* 25 (02), 162–170. doi:10.3969/j.issn.1672-9854.2020.02.008

Hu, M. Y., Cai, X. Y., Hu, Z. G., Qian, Y., and Xiang, J. (2009). Study on deep burial dissolution of Ordovician carbonate rocks in Tazhong area. *J. Oil Gas Technol.* 31 (06), 49–182. doi:10.3969/j.issn.1000-9752.2009.06.008

Husinec, A., and Jelaska, V. (2006). Relative Sea-level changes recorded on an isolated carbonate platform: tithonian to cenomanian succession, southern Croatia. *J. Sediment. Res.* 76 (10), 1120–1136. doi:10.2110/jsr.2006.099

Jia, P., Li, M., Lu, Y. Z., Fan, R., Li, X., Deng, S. H., et al. (2017). Sequence stratigraphic subdivision and establishment of sequence stratigraphic framework in the Cambrian Xixiangchi Group of Sichuan basin. *Geol. Sci. Technol. Inf.* 36 (02), 119–127. doi:10.3969/j.issn.1000-9752.2009.06.008

Jiang, H. C., Wen, L., Zhou, G., Liang, J. T., He, Y., Liu, S. B., et al. (2023). Rare earth elements characteristics and diagenetic fluids of dolomites in the Longwangmiao Formation, eastern Sichuan Basin. *Nat. Gas. Geosci.* 34 (7), 1187–1202. doi:10.11764/j.issn.1672-1926.2023.02.013

Jiang, W. J., Hou, M. C., Xing, F. C., Xu, F. L., and Lin, L. B. (2016a). Diagenetic characteristics of dolomites in the cambrian loushanguan Group in southeastern Sichuan Basin. *Petroleum Geol. and Exp.* 38 (03), 311–319. doi:10.3969/j.issn.1673-8926.2016.05.005

Jiang, W. J., Hou, M. C., Xing, F. C., Xu, F. L., and Lin, L. B. (2016b). Characteristics and indications of rare earth elements in dolomite of the cambrian loushanguan Group,SE Sichuan Basin. *Oil and Gas Geol.* 37 (04), 473–482. doi:10.11743/ogg20160403

Jiang, X. Q., Guan, H. L., Liu, G. X., Li, J. M., Luo, K. P., Yan, J. X., et al. (2015). Diagenesis of middle and upper cambrian loushanguan Group reservoirs in nanchuan area,Sichuan Basin. *Petroleum Geol. and Exp.* 37 (03), 314–319. doi:10.11781/sysydz201503314

Jing, P., Huang, J. L., Bai, C. G., Chen, Z. Y., Xu, F. G., Chen, Y. M., et al. (2016). The present research situation of sequence and sedimentary facies of Xixiangchi Formation of Sichuan Basin. *Shandong Chem. Ind.* 45 (11), 65–66+69. doi:10.3969/j.issn.1008-021X.2016.11.026

Jiu, B., Huang, W. H., and Li, Y. (2020). The effect of hydrothermal fluids on ordovician carbonate rocks, southern ordos basin, China. *Ore Geol. Rev.* 126, 103803. doi:10.1016/j.oregeorev.2020.103803

Kaufman, J., Hanson, G. N., and Meyers, W. J. (1991). Dolomitization of the devonian swan hills formation, Rosevear field, Alberta, Canada. *Sedimentology* 38 (1), 41–66. doi:10.1111/j.1365-3091.1991.tb01854.x

Khaled, L., Marzouk, L., Moez, B. F., Ramla, B. R., and Taher, Z. (2020). Sedimentary and structural setting of the Aptian reservoir deposits in the Kasserine area, west-central Tunisia. *Geol. Croat.* 73 (1), 59–67. doi:10.4154/gc.2020.06

Land, L. S. (1985). The origin of massive dolomite. *J. Geolological Educ.* 33, 112–125. doi:10.5408/0022-1368-33.2.112

Lei, H. J., Li, G. R., Gao, Y. W., Zhou J, L., Feng, Y. Y., Fu, H., et al. (2016). Geochemical characteristics and generation mechanism of cambrian dolomite in the south of Sichuan Basin. *Mar. Orig. Pet. Geol.* 21 (03), 39–47. doi:10.3969/j.issn.1672-9854.2016.03.005

Li, J., and He, D. (2014). Palaeogeography and tectonic-depositional environment evolution of the Cambrian in Sichuan Basin and adjacent areas. *J. Of Palaeogeogr.* 16 (04), 441–460. doi:10.7605/gdlxb.2014.04.037

Li, L., Tan, X. C., Xia, J. W., Luo, B., and Chen, J. S. (2008). Influences of eustatic movement on the cambrian reservoirs of bank facies in Weiyuan gasfield the Sichuan Basin. *Nat. Gas. Ind.* (04), 19–21+135. doi:10.11698/PED.2013.03.10

Li, L. P., Liang, J. T., Liu, S. B., Guo, Y. B., Li, K. Y., He, Y., et al. (2022). Diagenesis and pore evolution of dolomite reservoirs of cambrian Xixiangchi Formation in central Sichuan Basin. *Lithol. Reserv.* 34 (3), 39–48. doi:10.12108/yxyqc.20220304

Li, W., Fan, R., Jia, P., Lu, Y. Z., Zhang, Z. J., Li, X., et al. (2019a). Sequence stratigraphy and lithofacies paleogeography of middle–upper cambrian Xixiangchi Group in Sichuan Basin and its adjacent area, SW China. *Petroleum Explor. Dev.* 46 (2), 226–240. doi:10.11698/PED.2019.02.04

Li, W. Z., Zhang, J. Y., Hao, Y., Ni, C., Tian, H., Zeng, Y. Y., et al. (2019b). Characteristics ol carbon and oxvgen isotopic, paleoceanographic environment and their relationship witreservoirs of the Xixiangchi Formation, southeastern Sichuan basin. *Acta Geol. Sin.* 93 (2), 487~500. doi:10.3969/j.issn.0001-5717.2019.02.015

Li, W. Z., Zhou, J. G., Zhang, J. Y., Hao, Y., Zeng, Y. Y., Ni, C., et al. (2016). Main controlling factors and favorable zone distribution of Xixiangchi Formation reservoirs in the Sichuan Basin. *Nat. Gas. Ind.* 36 (01), 52–60. doi:10.3787/j.issn.1000-0976.2016.01.006

Liang, J. T., Liu, S. B., Li, L. P., Dai, J., Li, X. T., and Mou, C. L. (2022). Geochemical constraints on the hydrothermal dolomitization of the middle-upper cambrian Xixiangchi Formation in the Sichuan Basin, China. *Front. Earth Sci.* 10, 927066. doi:10.3389/feart.2022.927066

Lin, Y., Chen, C., Shan, S. J., Zeng, Y. Y., Liu, X., Chen, Y. L., et al. (2017). Reservoir characteristics and main controlling factors of the Cambrian Xixiangchi Formation in the Sichuan Basin. *J. Pet. Geol. Exp.* 39 (5), 610–617. doi:10.11781/sysydz201705610

Liu, D. W., Cai, C. F., Hu, Y. J., Hu, Y. J., Jiang, L., Peng, Y. Y., et al. (2020). Multi-stage dolomitization process of deep burial dolostones and its influence on pore evolution:A case study of Longwangmiao formation in the Lower Cambrian of central Sichuan Basin. *J. China Univ. Min. and. Technol.* 49(6), 1150–1165. doi:10.13247/j.cnki.jcumt.001181

Luczaj, J. A. (2006). Evidence against the Dorag (mixing-zone) model for dolomitization along the Wisconsin arch—a case for hydrothermal diagenesis. *AAPG Bull.* 90 (11), 1719–1738. doi:10.1306/01130605077

Luo, P., Zhang, J., Liu, W., Song, J. M., Zhou, G., Sun, P., et al. (2008). Characteristics of marine carbonate hydrocarbon reservoirs in China. *Earth Sci. Front.* 15 (01), 36–50. doi:10.3321/j.issn:1005-2321.2008.01.004

Ma, F. (2011). The summary on exploration of the dolomite oilfields in the world. *Acta Sedimentol. Sin.* 29 (5), 1010–1021. doi:10.14027/j.cnki.cjxb.2011.05.014

Machel, H. G. (2004). "Concepts and models of dolomitization: a critical reappraisal," in *The geometry and petrogenesis of dolomite hydrocarbon reservoirs*. Editors C. J. R. Braithwaite, G. Rizzi, and G. Darke (London, United Kingdom: Geological Society, London, Special Publications), 7–63. doi:10.1144/GSL.SP.2004.235.01.02

Manche, C. J., and Kaczmarek, S. E. (2019). Evaluating reflux dolomitization using a novel high-resolution record of dolomite stoichiometry: a case study from the Cretaceous of central Texas, USA. *Geology* 47 (6), 586–590. doi:10.1130/g46218.1

McCrea, J. M. (1950). On the isotopic chemistry of carbonates and paleotemperature scale. *J. Chem. Phys.* 18, 849–857. doi:10.1063/1.1747785

Meyera, W. J., Lu, F. H., and Zachariah, J. K. (1997). Dolomitization by mixed evaporative brines and freshwater, upper Miocene carbonates, Nijar, Spain. *J. Sed imentary Res.* 67 (5), 898–912. doi:10.1306/D4268671-2B26-11D7-8648000102C1865D

Morrow, D. W. (2014). Zebra and boxwork fabrics in hydrothermal dolomites of northern Canada: indicators for dilational fracturing, dissolution or *in situ* replacement? *Sedimentology* 61 (4), 915–951. doi:10.1111/sed.12094

Nothdurft, L. D., Webb, G. E., and Kamber, B. S. (2004). Rare earth element geochemistry of Late Devonian reefal carbonates, Canning Basin, Western Australia: confirmation of a seawater REE proxy in ancient limestones. *Geochimica Cosmochimica Acta* 68 (2), 263–283. doi:10.1016/s0016-7037(03)00422-8

Özyurt, M., Demir, Y., Özkan, K., and Kandemir, R. (2023). Geochemistry of the lake sediments on robert island, south shetland islands, Antarctica: implications for weathering processes in polar areas. *Turkish J. Earth Sci.* 32 (8), 944–960. Article 2. doi:10.55730/1300-0985.1885

Özyurt, M., and Kırmacı, M. Z. (2025). Microfacies and geochemistry of Kimmeridgian limestone strata in the Eastern Pontides (North-East Turkey): palaeoclimate and palaeoenvironmental influence on organic matter enrichment. *Depositional Rec.* 11, 4–21. doi:10.1002/dep2.286

Özyurt, M., Kırmacı, M. Z., Al-Aasm, I., Hollis, C., Taslı, K., and Kandemir, R. (2020). REE characteristics of lower cretaceous limestone succession in gümüşhane, NE Turkey: implications for ocean paleoredox conditions and diagenetic alteration. *Minerals* 10 (8), 683. doi:10.3390/min10080683

Özyurt, M., Kırmacı, M. Z., and Al-Aasm, I. S. (2019). Geochemical characteristics of Upper Jurassic – lower Cretaceous platform carbonates in Hazine Mağara, Gümüşhane (northeast Turkey): implications for dolomitization and recrystallization. *Can. J. Earth Sci.* 56 (3), 306–320. doi:10.1139/cjes-2018-0168

Parsapoor, A., Khalili, M., and Mackizadeh, M. A. (2009). The behaviour of trace and rare earth elements (REE) during hydrothermal alteration in the Rangan area (Central Iran). *J. Asian Earth Sci.* 34 (2), 123–134. doi:10.1016/j.jseaes.2008.04.005

Peng, B., Li, G., Li, Z., Liu, C., Zuo, Y., Zhang, W., et al. (2018). Discussion of multiple formation mechanisms of saddle dolomites—comparison of geochemical data of Proterozoic–Paleozoic dolomites. *Energy Explor. and Exploitation* 36 (1), 66–96. doi:10.1177/0144598717728464

Qing, H. R., and Mountjoy, E. W. (1994). Formation of coarsely crystalline, hydrothermal dolomite reservoirs in the Presqu'ile Barrier, Western Canada Sedimentary Basin. *AAPG Bull.* 78 (1), 55–77. doi:10.1306/bdff9014-1718-11d7-8645000102c1865d

Ren, G. X., Qin, Q. R., Qin, Z. J., Guo, Y. B., and Ye, Z. Y. (2022). Effects of diagenesis on quality of deep dolomite reservoirs: a case study of the Upper Cambrian Xixiangchi Formation in the eastern Sichuan Basin, China. *Front. Earth Sci.* 10, 984463. doi:10.3389/feart.2022.984463

Roehl, P. O., and Choquette, P. W. (1985). P. O. Roehl and P. W. Choquette (eds.). 1985. Carbonate petroleum reservoirs. Casebooks in earth science series. Xxii + 622 pp. Berlin, heidelberg, New York, Tokyo: springer-verlag. Price DM 220.00. ISBN 3 540 96012 0. *Geol. Mag.* 123 (6), 712–713. doi:10.1017/s0016756800024365

Ryan, B. H., Kaczmarek, S. E., and Rivers, J. M. (2020). Early and pervasive dolomitization by near-normal marine fluids: new lessons from an Eocene evaporative setting in Qatar. *Sedimentology* 67 (6), 2917–2944. doi:10.1111/sed.12726

Su, A., Chen, H. H., Feng, Y. X., Zhao, J. X., Wang, Z. C., Hu, M. Y., et al. (2022). *In situ* U-Pb dating and geochemical characterization of multi-stage dolomite cementation in the Ediacaran Dengying Formation, Central Sichuan Basin, China:Constraints on diagenetic, hydrothermal and paleo-oil filling events. *Precambrian Res.* 368, 106481. doi:10.1016/j.precamres.2021.106481

Sun, S. (1995). Dolomite reservoirs: porosity evolution and reservoir characteristics. *AapgBulletin* 79 (2), 186–204. doi:10.1306/8d2b14ee-171e-11d7-8645000102c1865d

Tucker, M. E., and Wright, V. P. (1990). *Carbonate sedimentology*. Oxford, UK: Blackwell Publishing.

Veizer, J., Ala, D., Azmy, K., Bruckschen, P., Buhl, D., Bruhn, F., et al. (1999). 87Sr/86Sr, $\delta^{13}C$ and $\delta^{18}O$ evolution of Phanerozoic seawater. *Chem. Geol.* 161 (1-3), 59–88. doi:10.1016/s0009-2541(99)00081-9

Wang, L. C. (2015). *A study of geochemical tracers for fluids related to d olomite reservoirs*. Nanjing, China: Nanjing University. [master's thesis]. doi:10.12108/yxyqc.20190205

Wang, L. J. (2019). Characteristics and controlling factors of high quality reservoirs of the fourth member of Dengying Formation in northern Sichuan Basin. *Lithol. Reserv.* 31 (2), 35–45.

Wang, S. F., Wei, L., Zhang, F., and Wang, X. Z. (2008). Developmental mechanism of advantageous Xixiangchi Group reservoirs in Leshan-Longnüsi palaeohigh. *Pet. Explor. Dev.* 35 (2), 170–174. doi:10.1016/S1876-3804(08)60023-3

Warren, J. (2000). Dolomite: occurrence, evolution and economically important associations. *Earth-Science Rev.* 52 (1-3), 1–81. doi:10.1016/s0012-8252(00)00022-2

Webb, G. E., and Kamber, B. S. (2000). Rare earth elements in Holocene reefal microbialites: a new shallow seawater proxy. *Geochimica Cosmochimica Acta* 64 (9), 1557–1565. doi:10.1016/s0016-7037(99)00400-7

Wen, H. G., Liang, J. T., Zhou, G., Qiu, Y. C., Liu, S. B., Li, K. Y., et al. (2022). Sequence-based lithofacies paleogeography and favorable natural gas exploration areas of Cambrian Xixiangchi Formation in Sichuan Basin and its periphery. *Lithol. Reserv.* 34 (2), 1–16. doi:10.12108/yxyqc.20220201

Xiong, J. B., and He, D. F. (2022). Distribution characteristics and controlling factors of global giant carbonate stratigraphic-lithologic oil and gas fields. *Lithol. Reserv.* 34 (1), 187–200. doi:10.12108/yxyqc.20220119

Zhang, P. Y., Wang, Y. L., Zhang, X. J., Wei, Z. F., Wang, G., Zhang, T., et al. (2022). Carbon, oxygen and strontium isotopic and elemental characteristics of the Cambrian Longwangmiao Formation in South China: paleoenvironmental significance and implications for carbon isotope excursions. *Gondwana Res.* 106, 174–190. doi:10.1016/j.gr.2022.01.008

Zhao, A. W., Tan, X. C., Li, L., Luo, B., Hong, H. T., Liu, J. W., et al. (2015). Characteristics and distribution of grain banks in the cambrian Xixiangchi Group of Sichuan Basin and its adjacent areas. *J. Of Palaeogeoeraphy* 17 (01), 21–32. doi:10.7605/gdlxb.2015.01.002

Zhao, M. Y., and Zhen, Y. F. (2017). A geochemical framework for retrieving the linked depositional and diagenetic histories of marine carbonates. *Earth Planet. Sci. Lett.* 460, 213–221. doi:10.1016/j.epsl.2016.11.033

Zhao, Y. Y., Li, S. Z., Li, Da., Guo, L. L., Dai, L. M., and Tao, J. L. (2019). Rare earth element geochemistry of carbonate and its paleoenvironmental implications. *Geotect. Metallogenia* 43 (01), 141–16. doi:10.16539/j.ddgzyckx.2019.01.011

Zhao, Y. Y., Zheng, Y. F., and Chen, F. (2009). Trace element and strontium isotope constraints on sedimentary environment of Ediacaran carbonates in southern Anhui, South China. *Chem. Geol.* 265 (3-4), 345–362. doi:10.1016/j.chemgeo.2009.04.015

Zheng, T. (2019). *Reservoir studies of the cambrian loushanguan Group in the jinshayankong area of the south Sichuan Basin [master's thesis]*. Chengdu, China: Chengdu University of Technology.

Zhou, G., Yan, Z. H., Lei, D. C., Li, Q., Zhong, Y., Yan, W., et al. (2024). Genetic model of dolomite and its influence on development of high-quality carbonate reservoir. *Nat. Gas Explor. Dev.* 47 (1), 1–11. doi:10.12055/gaskk.issn.1673-3177.2024.01.001